NASA CONTRACTOR REPORT

NASA CR-1600

DEVELOPMENT OF UHV MEASUREMENTS

by Charles M. Gosselin and George A. Beitel

Prepared by
MIDWEST RESEARCH INSTITUTE
Kansas City, Mo. 64110
for Langley Research Center

NATIONAL AERONAUTICS AND SPACE ADMINISTRATION • WASHINGTON, D. C. • MAY 1970

NASA CR-1600

DEVELOPMENT OF UHV MEASUREMENTS

By Charles M. Gosselin and George A. Beitel

Issued by Originator as MRI Project No. 3266-C

Prepared under Contract No. NAS 1-8730 by
MIDWEST RESEARCH INSTITUTE
Kansas City, Mo. 64110

for Langley Research Center

NATIONAL AERONAUTICS AND SPACE ADMINISTRATION

For sale by the Clearinghouse for Federal Scientific and Technical Information
Springfield, Virginia 22151 – CFSTI price $3.00

PREFACE

The goal of this program has been to extend the lower pressure-measuring limits of the buried collector gauge and of the orbitron gauge. The program has been supported by NASA under Contract No. NAS1-8730. This report describes the research accomplished during the period 29 October 1968 through 26 November 1969.

The program was conducted in the Physics Section of the Midwest Research Institute under the direction of Mr. Gordon Gross, Section Head. Mr. Charles Gosselin and Dr. George Beitel have conducted the research program.

TABLE OF CONTENTS

TABLE OF CONTENTS (Continued)

List of Figures

TABLE OF CONTENTS (Concluded)

List of Figures (Concluded)

DEVELOPMENT OF UHV MEASUREMENTS

By

Charles M. Gosselin
and
George A. Beitel
Midwest Research Institute

I. INTRODUCTION

The object of vacuum technology is to provide evacuated environments in which to observe or control physical phenomena. Often the level of evacuation must be measured in order to characterize the environmental conditions. Pressure is the parameter most often used to describe levels of evacuation within a chamber. However, the concept of pressure is based on a macroscopic definition and below 1 x 10^{-5} torr has little conceptual significance. At or below such pressure it is more meaningful to measure the molecular gas density via ionization methods. Instruments for this purpose are generally called "total pressure ionization gauges."

Ideally, ionization gauges produce an electric current which is a well-defined function of the gas density within an evacuated region. This current is small in the ultrahigh vacuum range, and is often masked by background currents. In hot-filament ionization gauges, various effects are responsible for the generation of limiting background currents; among these effects are: (a) molecular and ionic desorption due to electron bombardment of the anode, (b) photoelectron emission from the ion collector due to soft x-rays which are produced by electron impact at the anode, (c) ion desorption from hot filaments, and (d) leakage currents--including capacitive and inductive coupling.

The purpose of the present work has been to develop and evaluate gauging techniques which can be used to improve the low-pressure response capabilities of ionization gauges. The types of gauges which have been studied during this program are the buried collector gauge (BCG), the full sized orbitron gauge and a small model of the orbitron gauge.

In general, two approaches can be used to extend the lower pressure-measuring limit of ionization gauges: modifications to gauge design or operating parameters, and data-processing techniques which are external to the gauge itself. In this work, we have used a combination of these techniques.

It is useful at this point to define three terms which are used throughout the report: gauge constant (β), gauge sensitivity (S), and low pressure index (LPI). The gauge constant (β) is defined by

$$\beta = \frac{I^+}{PI_e} \quad , \tag{1}$$

where I^+ is the current to the ion collector, I_e is the electron emission current and P is the pressure within the test chamber. The gauge sensitivity (S) is defined by

$$S = \frac{I^+}{P} = \beta I_e \quad . \tag{2}$$

The low pressure index (LPI) is defined as

$$LPI = \frac{i_r}{I^+/P} = \frac{i_r}{\beta I_e} \quad , \tag{3}$$

where i_r is the pressure independent residual background current to the ion collector.

If the low pressure operation limit of an ionization gauge is to be extended, the low pressure index value must be reduced. This reduction can be accomplished by either reducing the background current to the ion collector or by increasing the gauge sensitivity. However, the low-pressure index is the measure of the low-pressure response characteristics of the gauge; neither an increase in sensitivity which produces a proportional increase in residual currents nor a decrease in background current accompanied by a proportional decrease in sensitivity improves the low pressure response characteristics.

In addition to the development and evaluation of low-pressure gauging techniques, the present study has also been concerned with the utilization of existing technology to establish low-pressure norms. The latter work is covered in a section on gauge testing which follows the three sections on development of gauges.

II. BURIED COLLECTOR GAUGE DEVELOPMENT

The buried collector gauge is a recent development[1,2]* which is of considerable interest for ultrahigh-vacuum measurement. These gauges are still in the experimental stage and have been studied in detail on this project. An experimental buried collector gauge (EBCG No. 1) whose design of the gauge is similar to that proposed by Clay and Melfi[1,2] was built and evaluated. This unit incorporates similar dimensions to those used

* Numbers shown in this manner are references, which are shown on pp. 54-55.

by Melfi[2] (NASA, Langley Research Center) in the fabrication of the buried collector gauge No. 2 (BCG No. 2).

We have determined empirically the operating parameters for the EBCG No. 1 and have studied its response characteristics in the pressure range between 10^{-14} torr and 10^{-4} torr. It has been determined that the EBCG No. 1 is linear over at least eight decades of pressure, and that in a properly degassed gauge, the nonpressure-dependent background current to the ion collector is stable. The empirically determined operating parameters and zero-suppression techniques have been used for data collection at low pressure, and it has been thus established that this type gauge can be used for pressure measurements through the 10^{-12} torr range. If greater measurement uncertainty can be tolerated, the gauge can be used through the 10^{-13} torr range.

The vacuum system on which the EBCG No. 1 has been studied is a dynamic pressure ratio system[3] with a low- to high-pressure ratio of 1.4×10^{-3}. The test gas used - helium - is admitted via a vycor diffuser unit into the high pressure side of the ratio system. The pressure response data were taken by means of a pressure leak-up method; however, the pressure can be maintained at any desired value for an indefinite time by use of a Granville Phillips automatic-pressure controller valve located between the diffuser and the high-pressure side of the flow system. This capability allows steady-state conditions to be established before pressure readings are made. All data have been converted to torr (N_2) equivalent units using the relation

$$P_{N_2} = \frac{S_{N_2}}{S_{He}} P_{He} \quad , \tag{4}$$

where S_{He} and S_{N_2} are the sensitivities of Bayard-Alpert gauge for helium and nitrogen, respectively, and P_{He} is the measured pressure of helium. The value of $S_{He}/S_N = 0.16$ was used. The reference gauges were Bayard-Alpert gauges which had been calibrated previously.

A. Design of the Experimental Buried Collector Gauge

The experimental buried collector gauge (EBCG No. 1) is displayed schematically in Figure 1 and photographically in Figure 2. The gauge is mounted on a 2-3/4 in. O.D. ConFlat Flange into which a nine-pin electrical feedthrough has been welded. The gauge unit consists of six independent

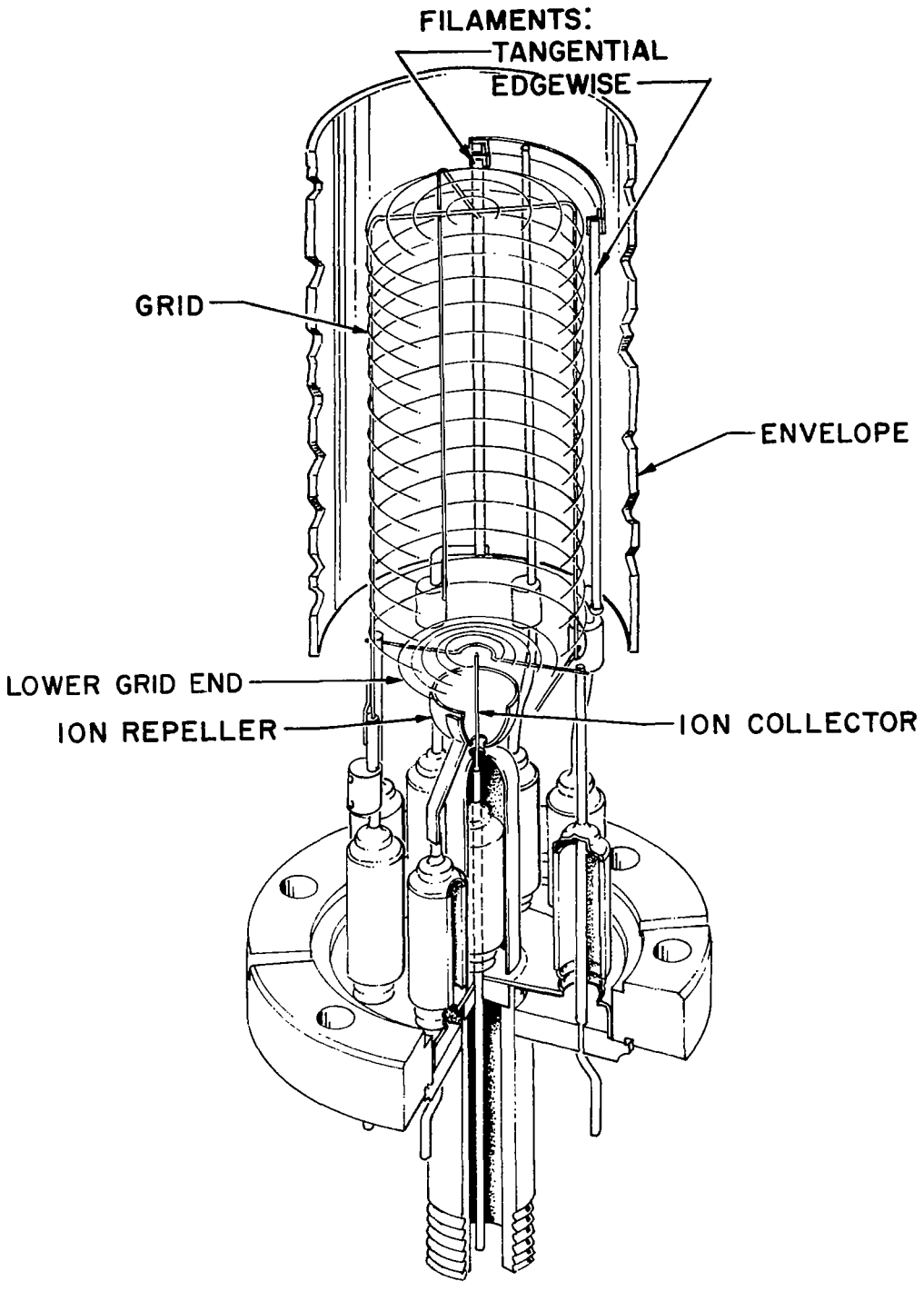

Figure 1 - Schematic of Experimental Buried Collector Gauge (EBCG). The lower grid end electrode is fabricated from small diameter concentric loops of wire attached to a low mass support.

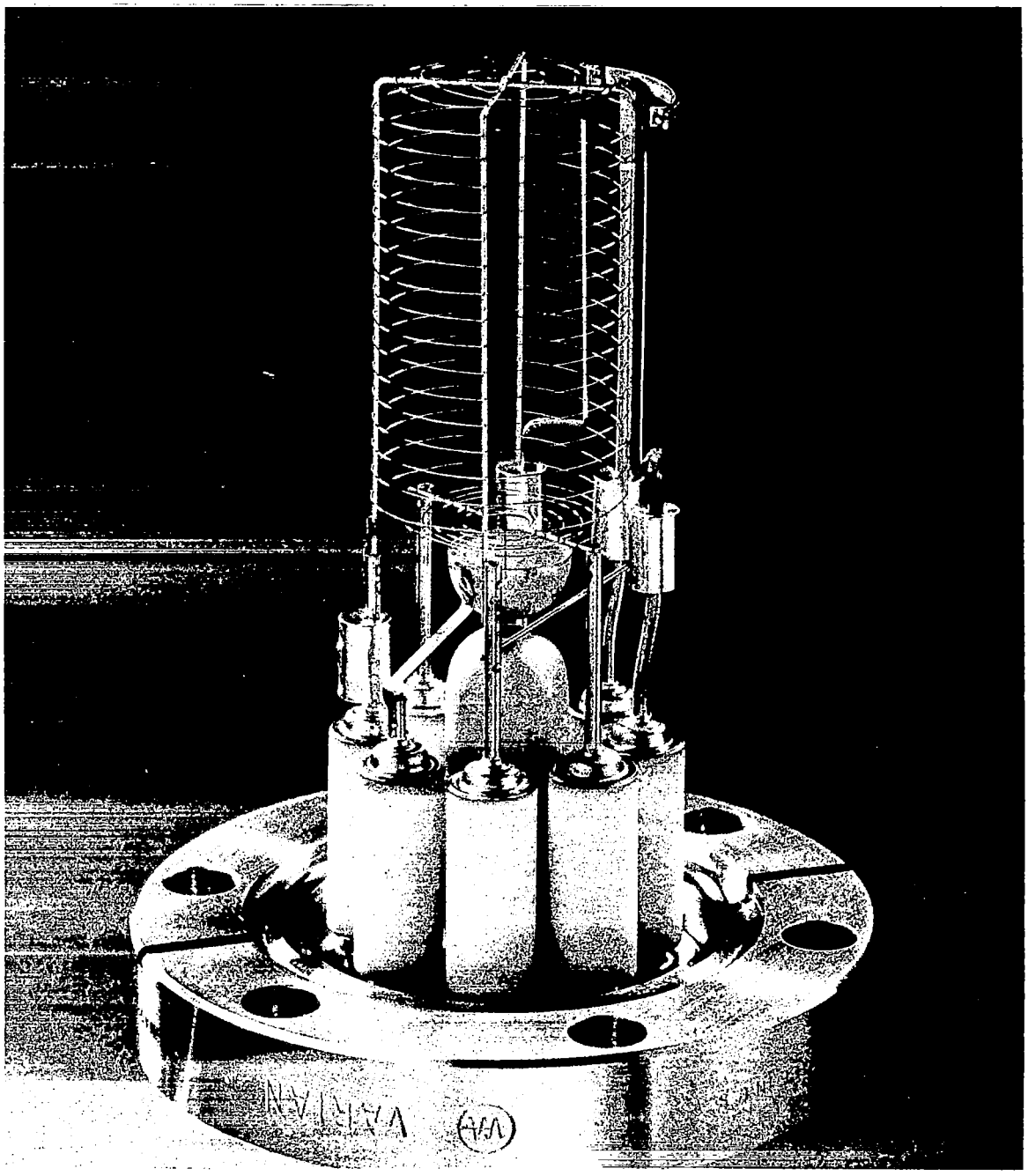

Figure 2 - Photograph of EBCG No. 1. The gauge is mounted on a nine-pin electrical-vacuum feedthrough and is equipped with two thoria coated iridium filaments.

electrodes, as is shown in Figure 1. The grid structure is a 2.54 cm. diameter helical coil, which is closed at the upper end. The lower grid end is a flat circular electrode fabricated from concentric loops of small diameter wire. This electrode is different from that used in the BCG No. 2 design:* it is not a solid annular ring. The ion collector, which is attached to the central electrical feedthrough, extends to the lower edge of the lower grid end electrode. A hemispherically shaped ion-repeller electrode surrounds the ion collector. This electrode is used to focus ions onto the ion collector. The gauge is equipped with two thoria-coated iridium ribbon filaments; one mounted edgewise to the grid, and one mounted tangent to the grid. A third filament (tungsten spiral) has also been employed in this study but is not shown in Figures 1 or 2.

B. Operating Parameters of the Experimental Buried Collector Gauge

The parameters with which the EBCG No. 1 was operated were determined by empirical techniques. Data collected from these studies are presented in Figures 3 to 8. Where possible, the gauge response is shown in terms of the gauge constant $\beta(N_2)$, defined by Eqs. (1) and (4).

Figures 3 and 4 show that the optimum relationship for the potentials of the filament (V_f), the lower grid end (V_{LGE}), and the envelope (V_B) is

$$V_f = V_B = V_{LGE}$$

---

* The primary purpose for the modified (i.e., reduced mass) lower grid end electrode design in the EBCG No. 1 is to permit high-temperature degassing of this electrode. The results of an earlier study under Contract NAS-7488[3] suggest that significant ionic desorption occurred at the shield electrode of the buried collector gauge, BCG No. 2.

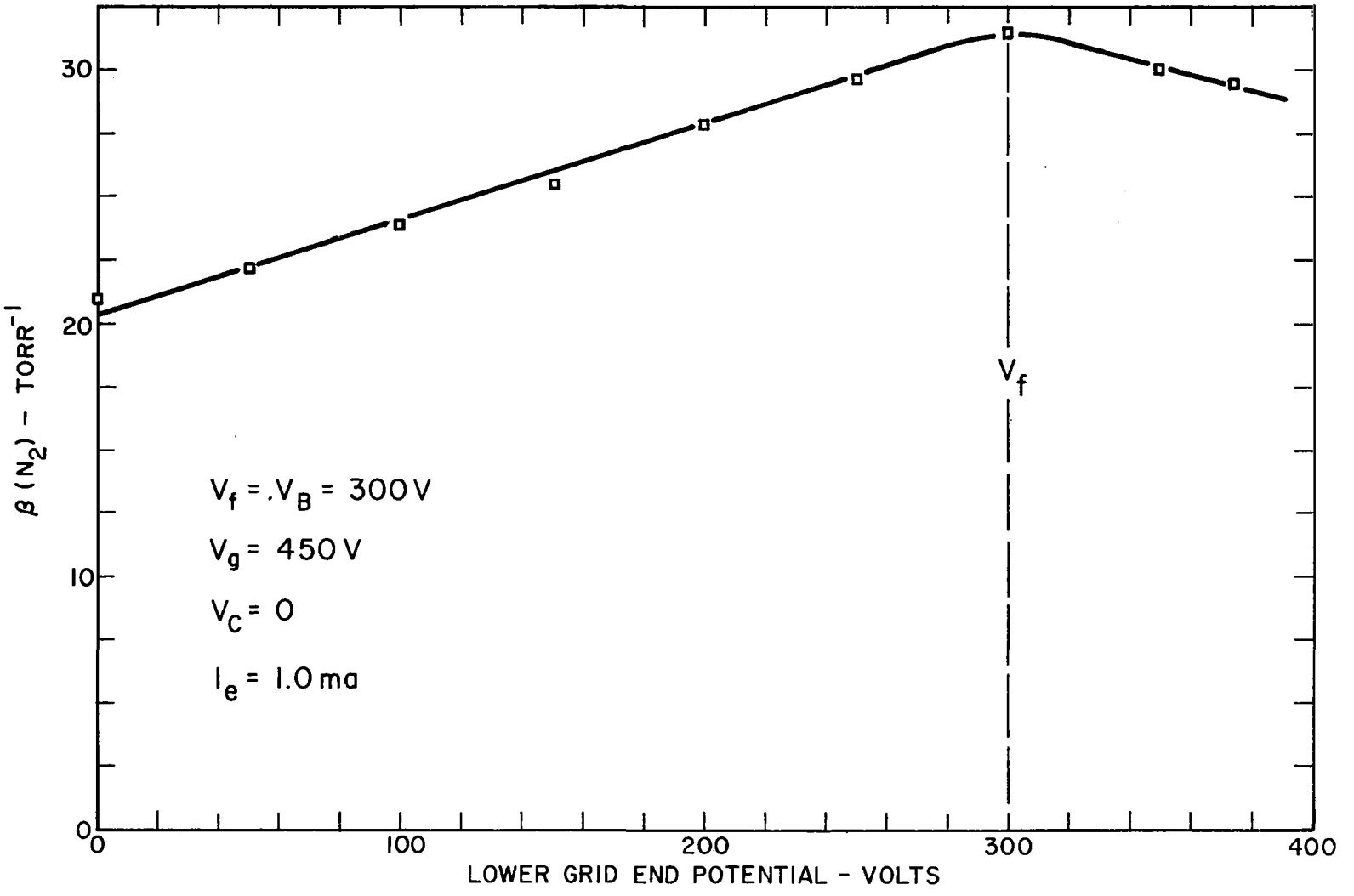

Figure 3 - Gauge Constant for Nitrogen Versus Lower Grid End Potential. The maximum value of $\beta(N_2)$ occurs for a lower grid end potential equal to the filament potential.

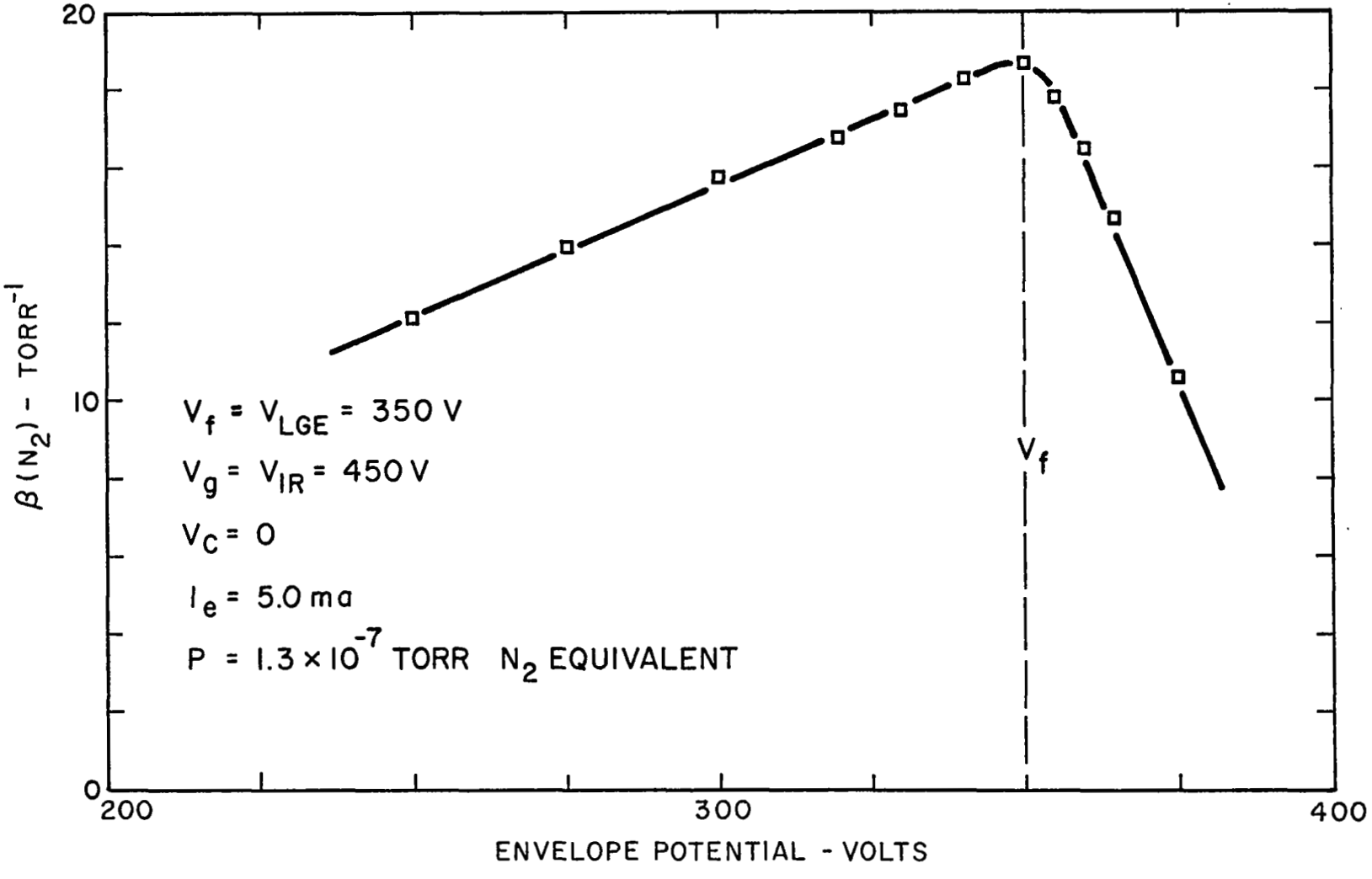

Figure 4 - Gauge Constant for Nitrogen Versus Envelope Potential. The maximum value of $\beta(N_2)$ occurs for an envelope potential equal to the filament potential.

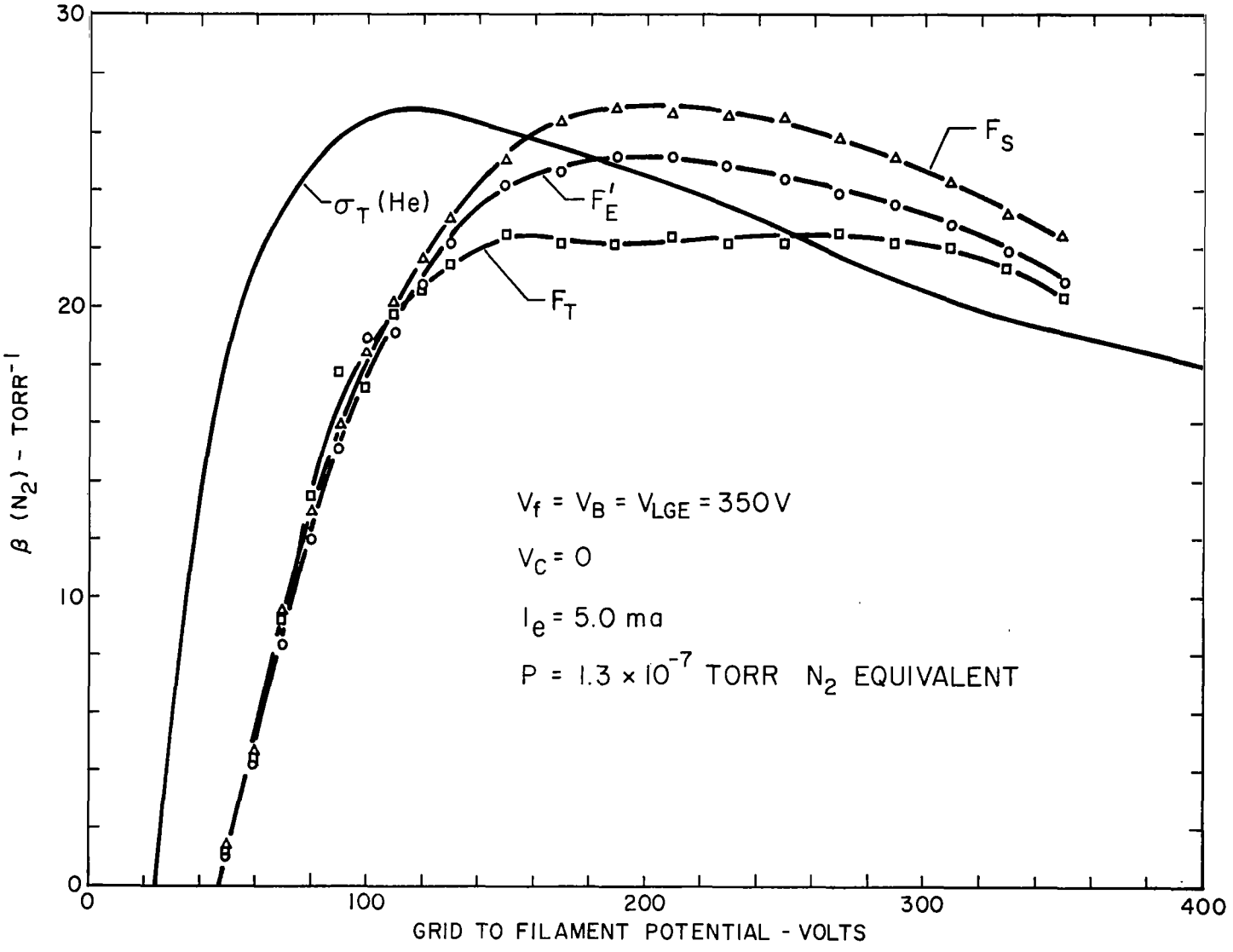

Figure 5 - Gauge Constant for Nitrogen Versus Grid to Filament Potential. The solid line is the total ionization cross section for helium (the test gas) versus the energy of bombarding electrons. The data in curves F_S , F_T , and F_E' were collected with helium gas.

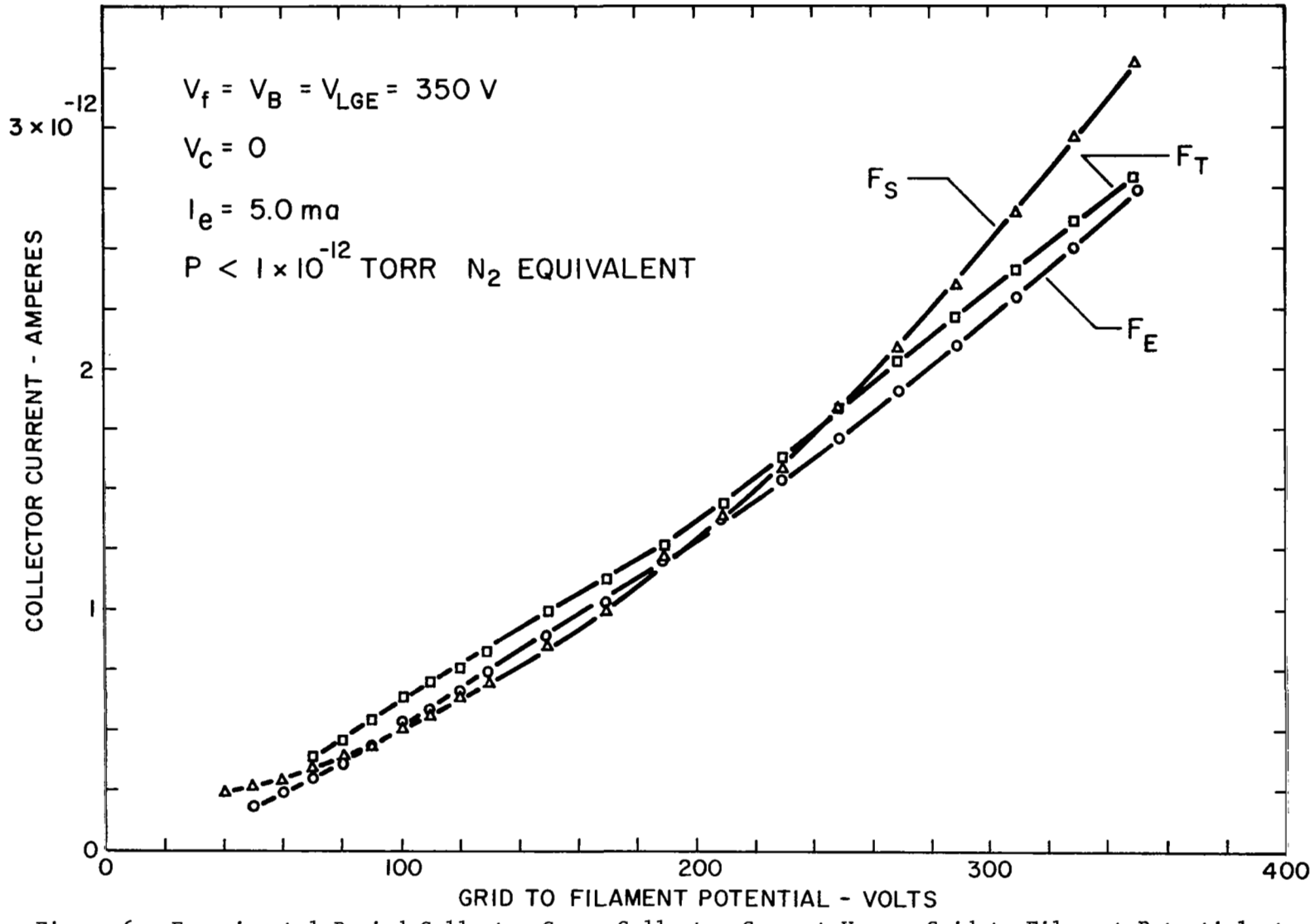

Figure 6 - Experimental Buried Collector Gauge Collector Current Versus Grid to Filament Potential at the Extreme Vacuum Limit. Monotonic increase in current as a function of electron energy indicates that the current is due to x-ray background.

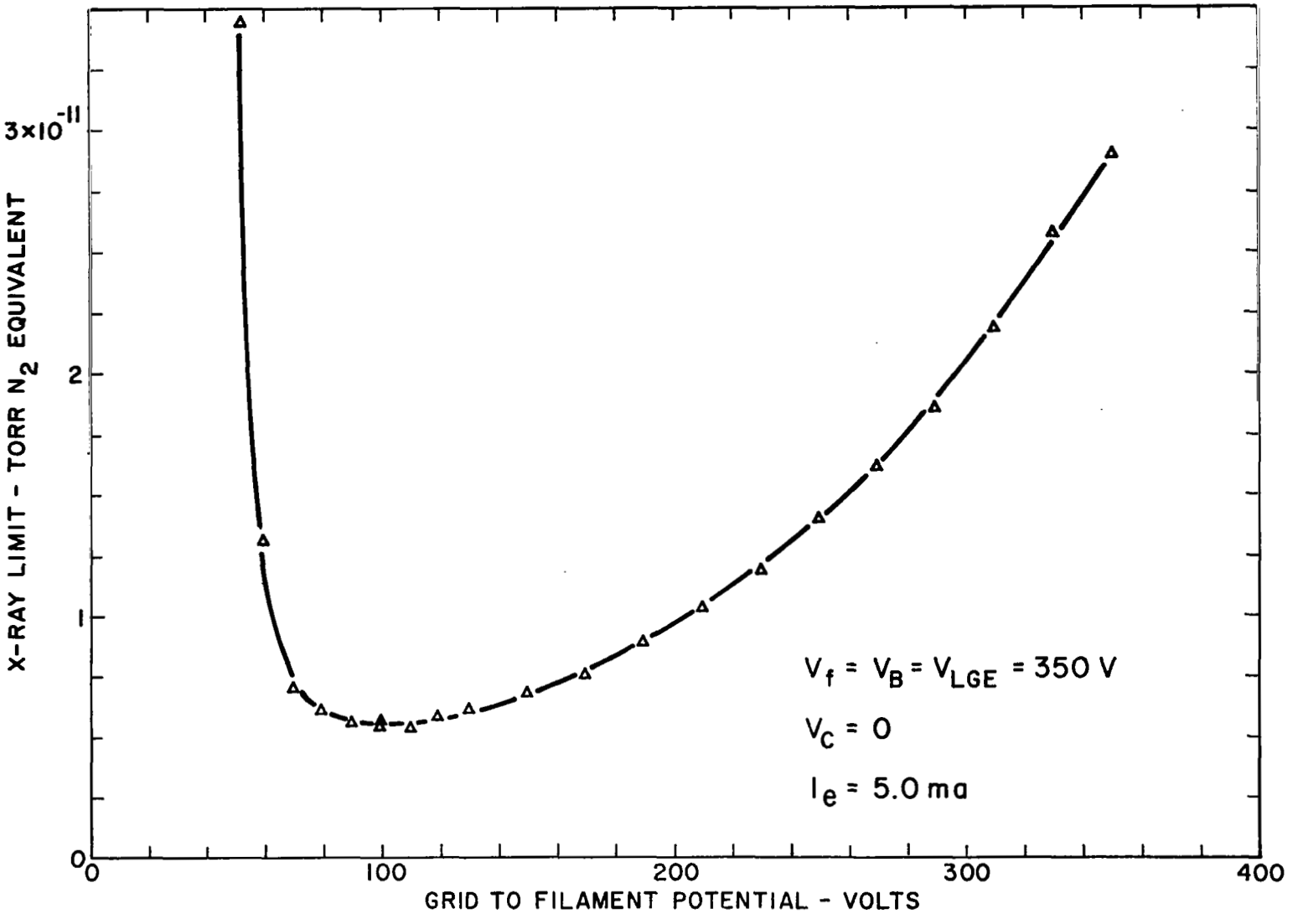

Figure 7 - X-ray Limit (low pressure index) Versus Grid to Filament Potential. The minimum value occurs for a grid to filament potential of about 100 V.

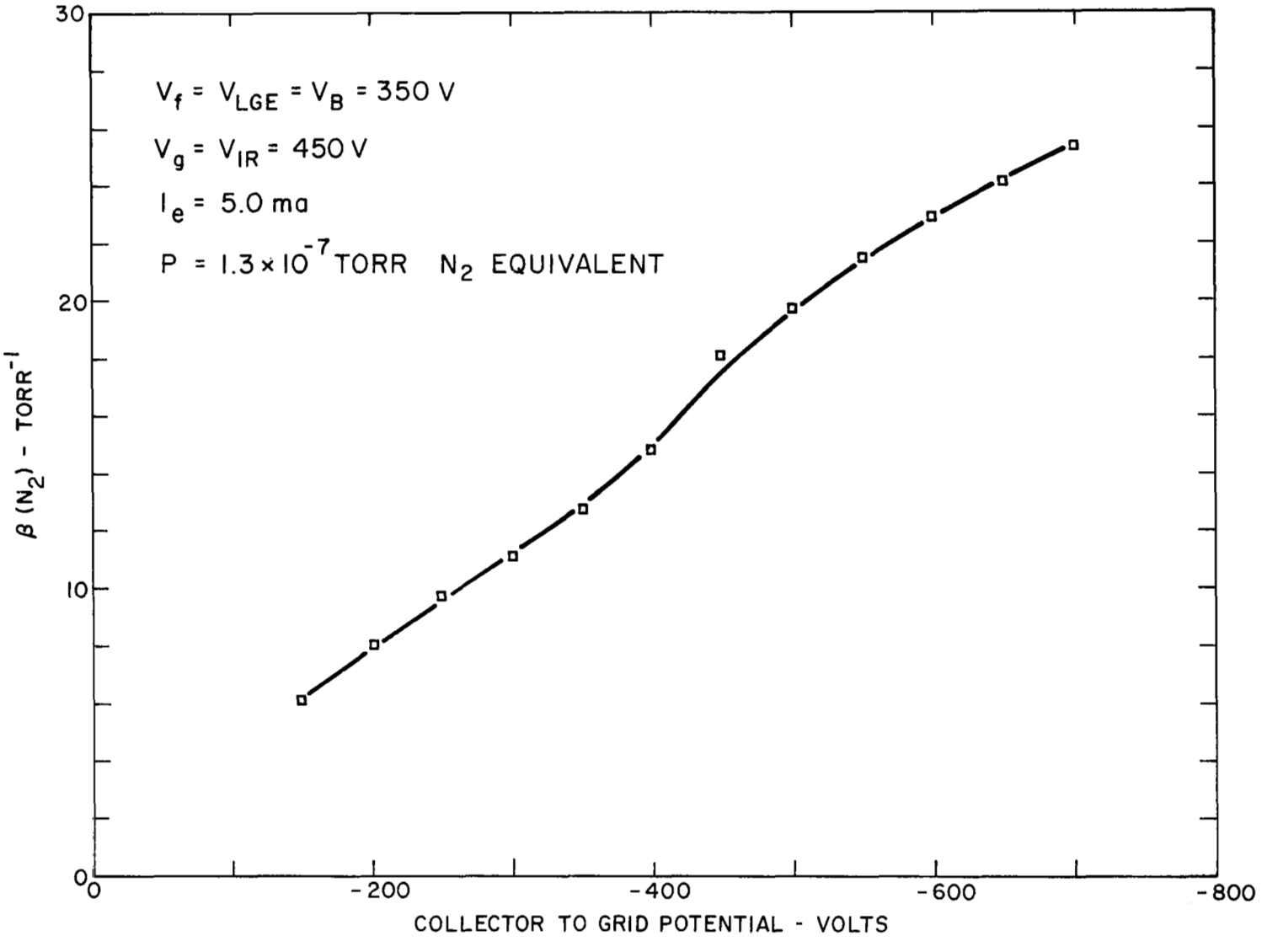

Figure 8 - Gauge Constant for Nitrogen Versus Collector to Grid Potential

Figure 5 displays the gauge constant $\beta(N_2)$ versus the grid to filament potential, measured at $P_{N_2} = 1.3 \times 10^{-7}$ torr . Three curves are shown labeled F_S , F_E' , and F_T . Each of the curves corresponds to a particular filament type and orientation which is discussed below. A fourth curve, $\sigma_T(He)$, is shown which corresponds to the total ionization cross section curve for electron bombardment of helium.[4] Although the experimental curves for the EBCG No. 1 do not exactly match the $\sigma_T(He)$ curve, there is good qualitative agreement. Variations are to be expected because of the complex field conditions which exist within a buried collector gauge grid volume, and $\beta(N_2)$ differs from $\sigma_T(He)$ by an unknown ion collection efficiency term. However, the shapes of the curves in Figure 5 indicate that the current which is measured at the ion collector electrode is due to ions generated in the gas phase.

The data in Figure 5 do not give adequate information to determine the best filament to grid potential for UHV operation. In addition to ion current, one must also consider background currents caused by soft x-rays produced by electron bombardment of the grid.

Figure 6 displays the pressure independent background current versus the grid to filament potential. A comparison of the shapes of the curves in Figures 5 and 6 clearly demonstrates that pressure-independent currents dominate the EBCG No. 1 response at pressures below 1×10^{-12} torr.

The data in Figures 5 and 6 have been combined to produce the curve shown in Figure 7. In this figure the pressure corresponding to a current which is equal to the x-ray photoelectron current (low pressure index, LPI) is plotted versus the grid to filament potential. The LPI is given by Eq. (3). The minimum in this curve occurs at a grid to filament potential of about 100 V. This voltage region is, therefore, preferred for UHV operation.

The data, Figure 8, show that the ion-collection efficiency increases with increasing collector to grid potential. Although improved performance may be obtained at higher collector to grid potentials, a value of +450 V is chosen because of electronic power supply considerations. It is convenient to operate the ion collector electrometer at ground potentials; therefore, by maintaining the grid at +450 V, the filament power supply is maintained at +350 V, which does not require an unusually high level of electrical isolation.

The ion-repeller electrode which is used to focus ions onto the ion collector is held at the grid potential (+450 V). This choice provides some discrimination between surface generated ions and gas generated ions.

Gas-generated ions are formed at potentials which are less than the grid potential and therefore cannot reach the ion repeller; instead, they are reflected onto the ion collector. The excess kinetic energy of ions desorbed from the surface of the grid permits them to be collected at the ion repeller electrode.

An emission current of 5.0 mA was chosen for this study. Although Figure 12, p. 19, indicates that, in general, larger gauge constants can be achieved at emission currents of $\sim$ 1.5 mA, the larger value of 5.0 mA was chosen to provide a gauge sensitivity S_{N_2} close to 0.1 A/torr, where

$$S_{N_2} = I^+/P_{N_2} = \beta(N_2) I_e \quad . \tag{5}$$

The six voltage-independent electrodes thus reduce to three (filament, grid, and ion collector), which is the same as a standard B.A. gauge. The only disadvantage over the B.A. gauge is the necessity of operating the grid at +450 V instead of +175 V. The additional gain in gauge constant which could be realized by operating at 1.5 mA emission is offset by the decrease in ion current signal.

C. Response of the Experimental Buried Collector Gauge

The response characteristics of the EBCG No. 1 have been determined: the ion current to pressure response, the gauge sensitivity to filament geometry variations, and outgassing characteristics.

1. Pressure response.-The pressure response of the EBCG No. 1 has been determined for two overlapping pressure ranges: 3×10^{-14} to 3×10^{-8} torr N_2 equivalent by comparison to a reference B.A. gauge via the pressure ratio technique, and 1×10^{-10} to 3×10^{-5} torr N_2 equivalent via direct comparison to a reference B.A. gauge. Figures 9 and 10 display these response curves. Data have been collected for three different filament conditions, as shown in Figure 11, where

Filament T is a thoria-coated iridium ribbon filament,

Filament E is a thoria-coated iridium ribbon filament, and

Filament S is a tungsten spiral filament.

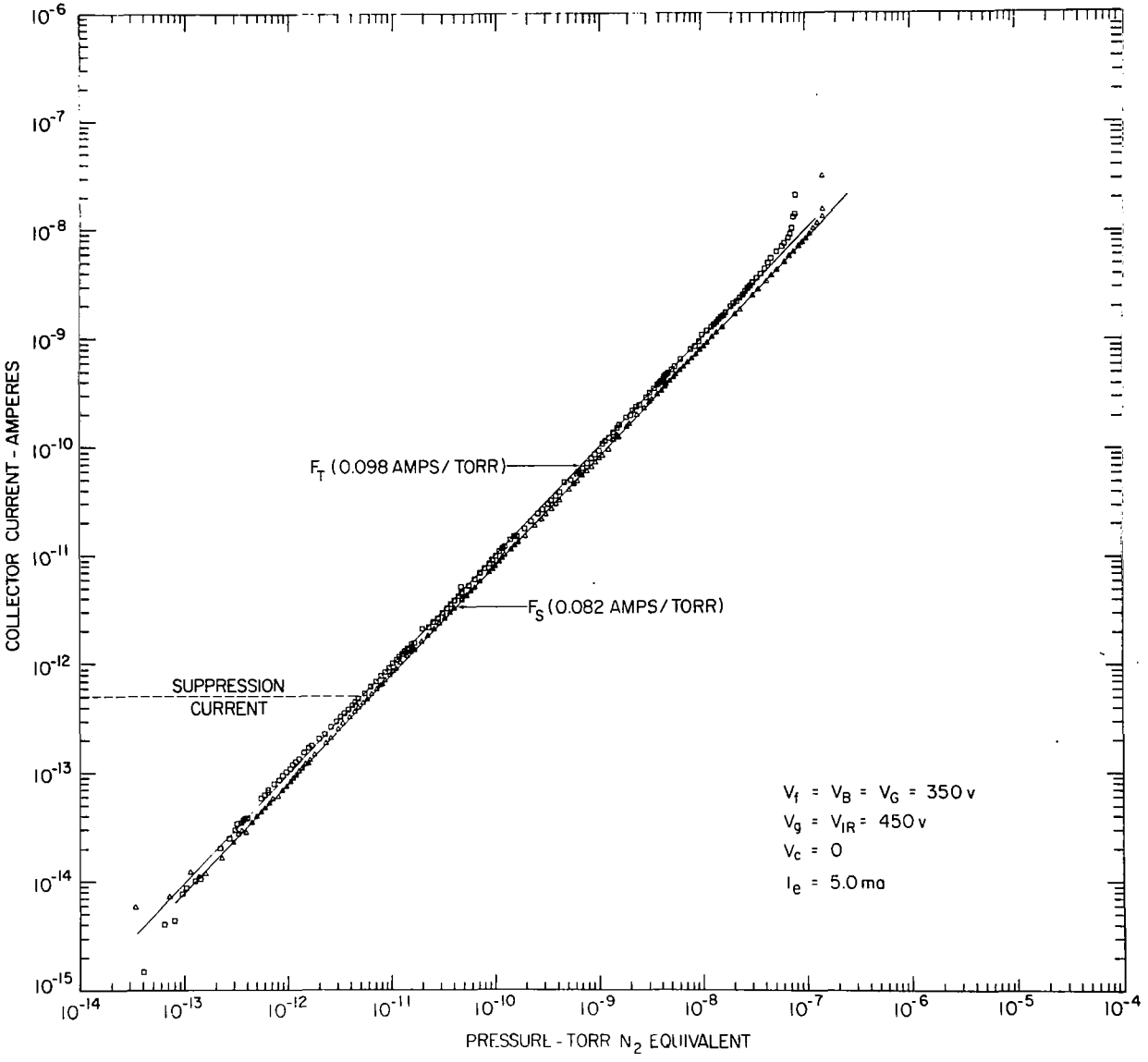

Figure 9 - Ion Collector Current of the EBCG Versus Pressure. A zero suppression current of 5.2×10^{-13} A was used and is indicated by the dashed line.

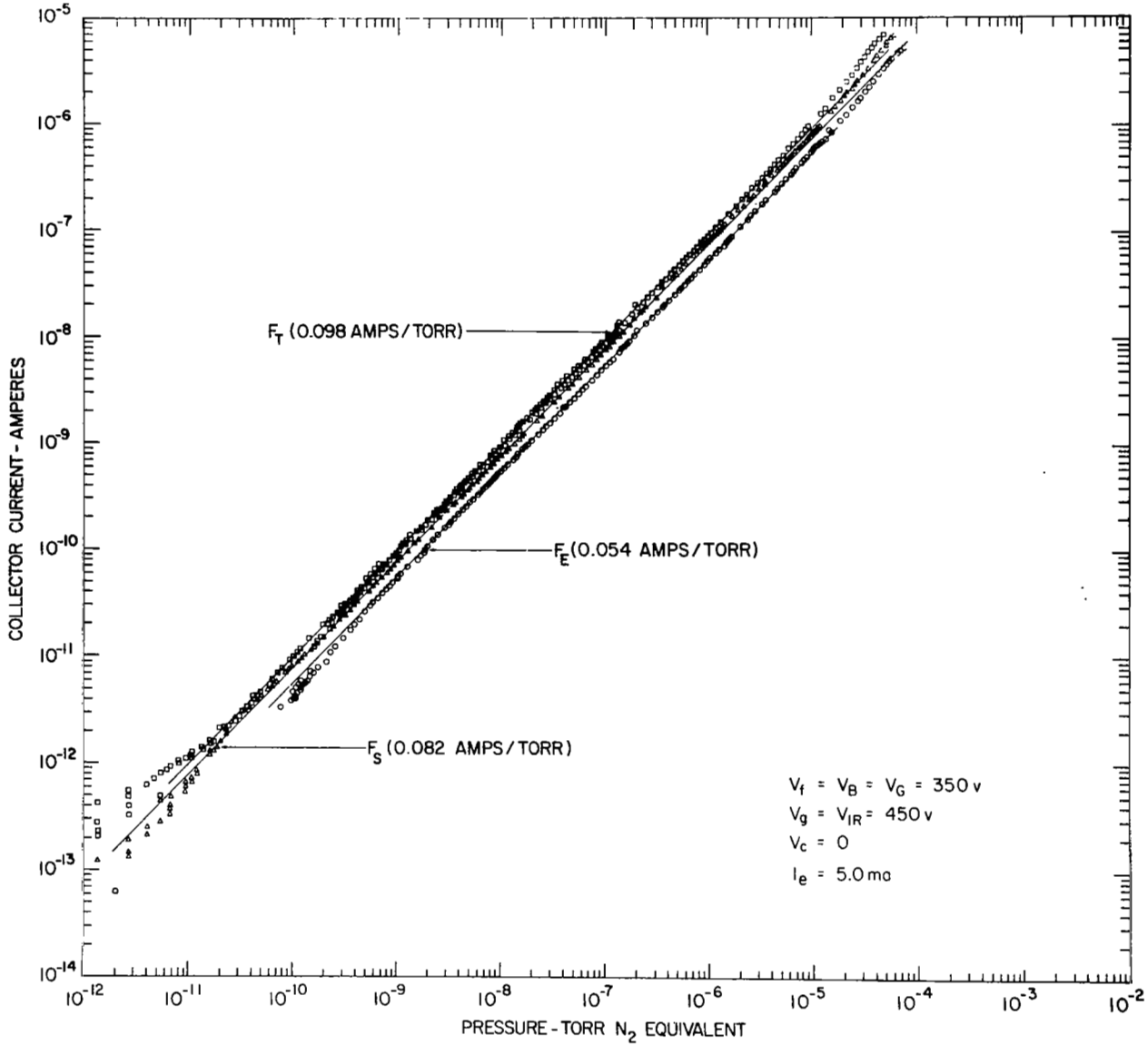

Figure 10 - Ion Collector Current of the EBCG Versus Pressure. The results for three different filaments are shown.

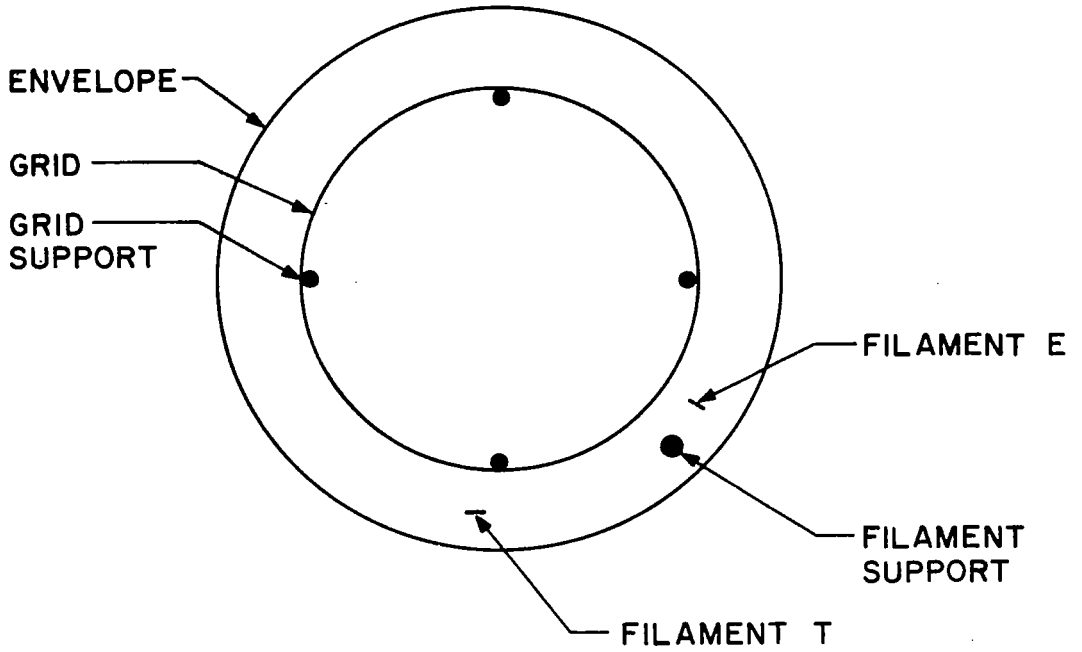

(a)

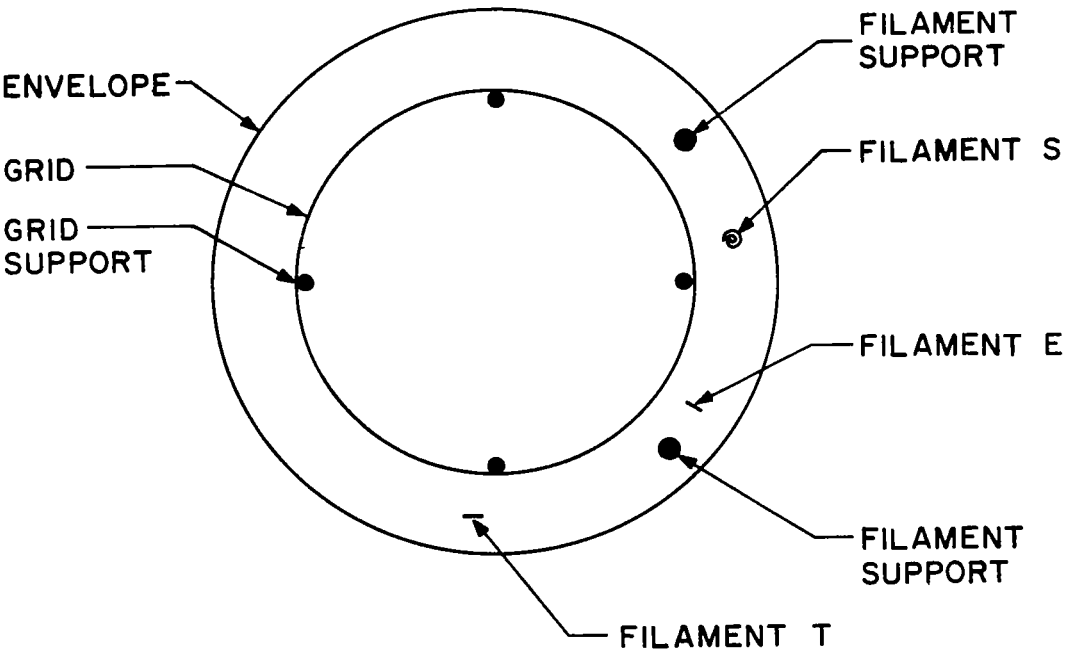

(b)

Figure 11 - Schematic Diagram of the End View of the EBCG. The geometry and orientation of the filaments, filament supports, grid, and envelope are shown.

The EBCG No. 1 has a linear response to pressure changes from 3×10^{-5} to 3×10^{-13} torr nitrogen equivalent. A background current of 5.2×10^{-13} A due to x-ray photoelectron current has been suppressed electronically during the measurement of ion current. The dashed line in Figure 9 indicates the level of zero suppression used.

The sharp break in the data in Figure 9 in the upper 10^{-8} torr N_2 equivalent range is due to the failure of the pressure ratio. This failure occurs because of a change in the pumping speed of the LHe cryopump which is used to evacuate the chamber in which the EBCG No. 1 is mounted. The pumping speed change is produced by saturation of the cryopump.

Linear response lines have been drawn through the data points for each filament condition, and the gauge sensitivity for each condition is given.

2. Filament parameters.-This section discusses the effects of filament configurations and emission current on the response of the EBCG. Four different configurations have been studied, and these are shown schematically in Figures 11a and b. The symbols in Table I are used to designate the various filament configurations and to identify the data presented in Figure 12.

TABLE I

SYMBOLS USED TO IDENTIFY FILAMENT CONFIGURATIONS IN THE EBCG

F_T - filament T of Figure 11a

F_E - filament E of Figure 11a

F_S - filament S of Figure 11b

F'_E - filament E of Figure 11b

F''_E - filament E of Figure 11a

The gauge constant $\beta(N_2)$ of the EBCG No. 1 as a function of emission current for the different filaments is shown in Figure 12. Although there is significant variance among the five curves, there are three common qualitative characteristics:

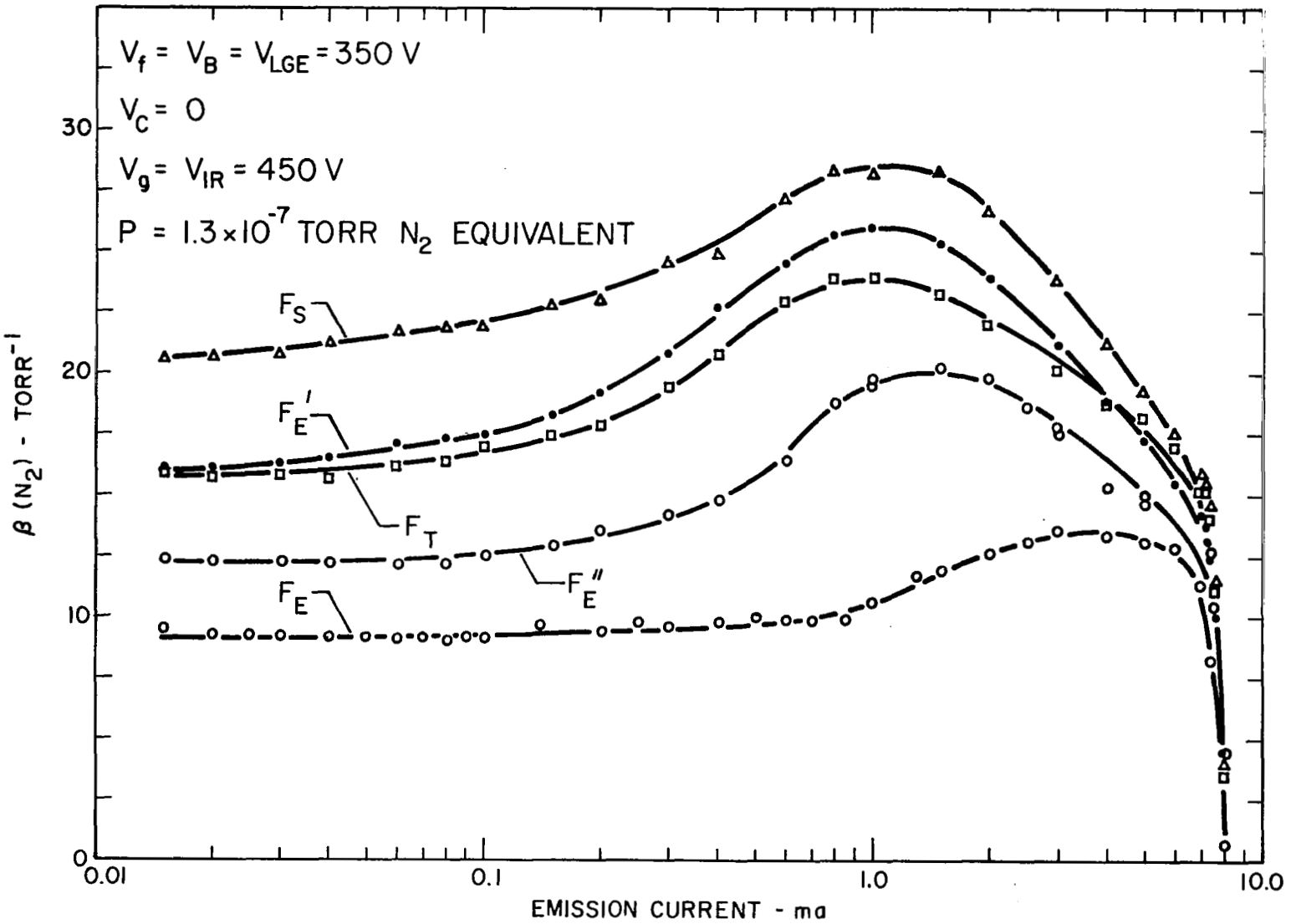

Figure 12 - Gauge Constant for Nitrogen Versus Emission Current. Data are presented for five filament conditions (see Table I).

1. Each curve indicates a flat response below 0.1 mA.
2. Each curve indicates a peaked response at $\sim$ 1 mA.
3. Each curve indicates a rapid fall-off in response beginning at $\sim$ 7 mA.

The region of flat response below 0.1 mA is characteristic of a response in which space charge effects are not significant. However, as the emission current is increased, the gauge constant begins a gradual increase. A speculative explanation for this increase is that, as space charge becomes appreciable, a greater fraction of the electrons is able to enter the grid volume at least once.* Thus, a greater level of ionization occurs, resulting in an increased gauge constant. Further increases in the emission current yield a peak gauge constant, followed by a gradual fall-off and then a very rapid fall-off. The fall-off in response is due to space charge limitation.

The differences in the curves of Figure 12 are of significant interest to warrant further discussion. The order in which the data were collected is helpful in interpreting the observed differences. The order was: obtain curve F_T and curve F_E, mount filament S, obtain curve F_S and curve F_E', remove filament S, and obtain curve F_E''.

The variations of $\beta(N_2)$ as a function of filament geometry are not entirely unexpected since the dependence of gauge constant upon the grid to filament spacing had been observed before.[5-7] The tangent to grid filament had a tendency to bow away from the grid, to such an extent that the hottest part of the filament, and consequently the region most active towards emission, was about 3 mm. from the grid. The edgewise-to-grid filament, even though it bowed when heated, always had its edge about 1.5 mm. from the grid. Nottingham[5] reported an increase in sensitivity of a factor of two in going from 1 mm. to 3 mm. grid to filament spacing. Our values are consistent with Nottingham's results.**

3. Outgassing.-The grid and lower grid end of the EBCG were outgassed by electron bombardment. A standard B.A. gauge control was employed for this procedure, since the outgassing power requirements were essentially the same as for a B.A. gauge. The reduced outgassing power requirement ($\sim$ 40 W) for the EBCG over the earlier buried collector gauge design tested in this laboratory[3] resulted from the replacement of the solid-disk lower

* A rough calculation gives a mean electron path length of 1.2 cm. The grid cage has a 2.4 cm. diameter; this implies that less than half the electrons ever enter the grid.

** Since this work was done, a paper by Redhead[8] has added to and helped clarify the question of gauge sensitivity variations as a function of filament location.

grid end with a low-mass spiral wire unit. No evidence of gas release from the EBCG was detected after outgassing.

D. Discussion

The modified buried collector gauge described here was shown to have an x-ray photoelectron current of 5.2×10^{-13} A when operated at 5.0 mA emission and a filament to grid potential of 100 V. This is in good agreement with the minimum current of 3.2×10^{-13} A when operated at 4.0 mA emission reported by Melfi.[2] The major advantage of constructing the lower grid end from a wire spiral, which replaces the solid shield of the original design, is the increased ease in outgassing. The EBCG is sufficiently similar to the standard B.A. gauge that no difficulties should be encountered in going to the EBCG design to achieve a reduction of one decade in the low pressure limit.

The background currents are sufficiently stable to permit dependable measurements down to the low 10^{-13} torr range. Finally, the disadvantage which was noted, i.e., gauge constant changes due to filament placement, may be overcome by proper filament design and, perhaps, gauge constants of 30 $torr^{-1}$ or better will be possible.

III. ORBITRON GAUGE DEVELOPMENT

This section discusses a continuing development program which was begun on a previous NASA contract.[3] The control orbitron gauge and the suppressor grid orbitron gauge which have been used in the present work were developed on that contract. The major concern of this research phase has been to determine the effects of anode diameter and filament position on the sensitivity and stability of the two orbitron gauges.

A. Orbitron Gauges

The orbitron gauge (COG) is shown schematically in Figure 13 and has been described in detail elsewhere.[3] The suppressor grid orbitron gauge (SGOG) is shown schematically in Figure 14 and photographically in Figure 15. The unique characteristics of the SGOG is that a 3.81 cm. diameter helical-coil electrode is located between the 4.76 cm. diameter solid ion collector and the anode. The helical coil is maintained at a negative potential with respect to the ion collector and, therefore, acts as a suppressor grid for secondary electron emission from the ion collector.

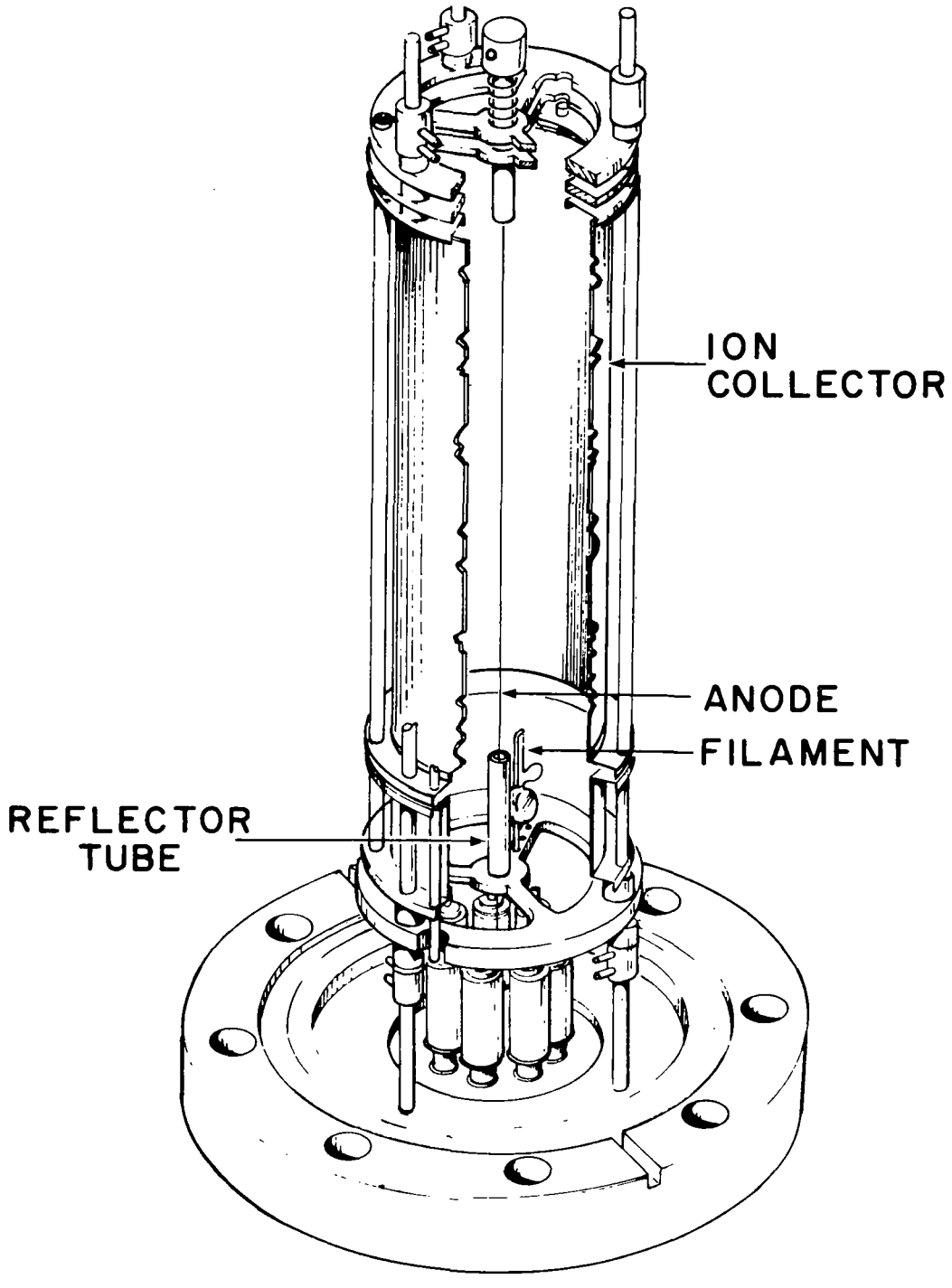

Figure 13 - Diagram of Control Orbitron Gauge (COG). The cathodes are mounted on three ceramic rods. The filament assembly is shown at the 0.3R position. The central anode is held tight by a tungsten spiral spring assembly.

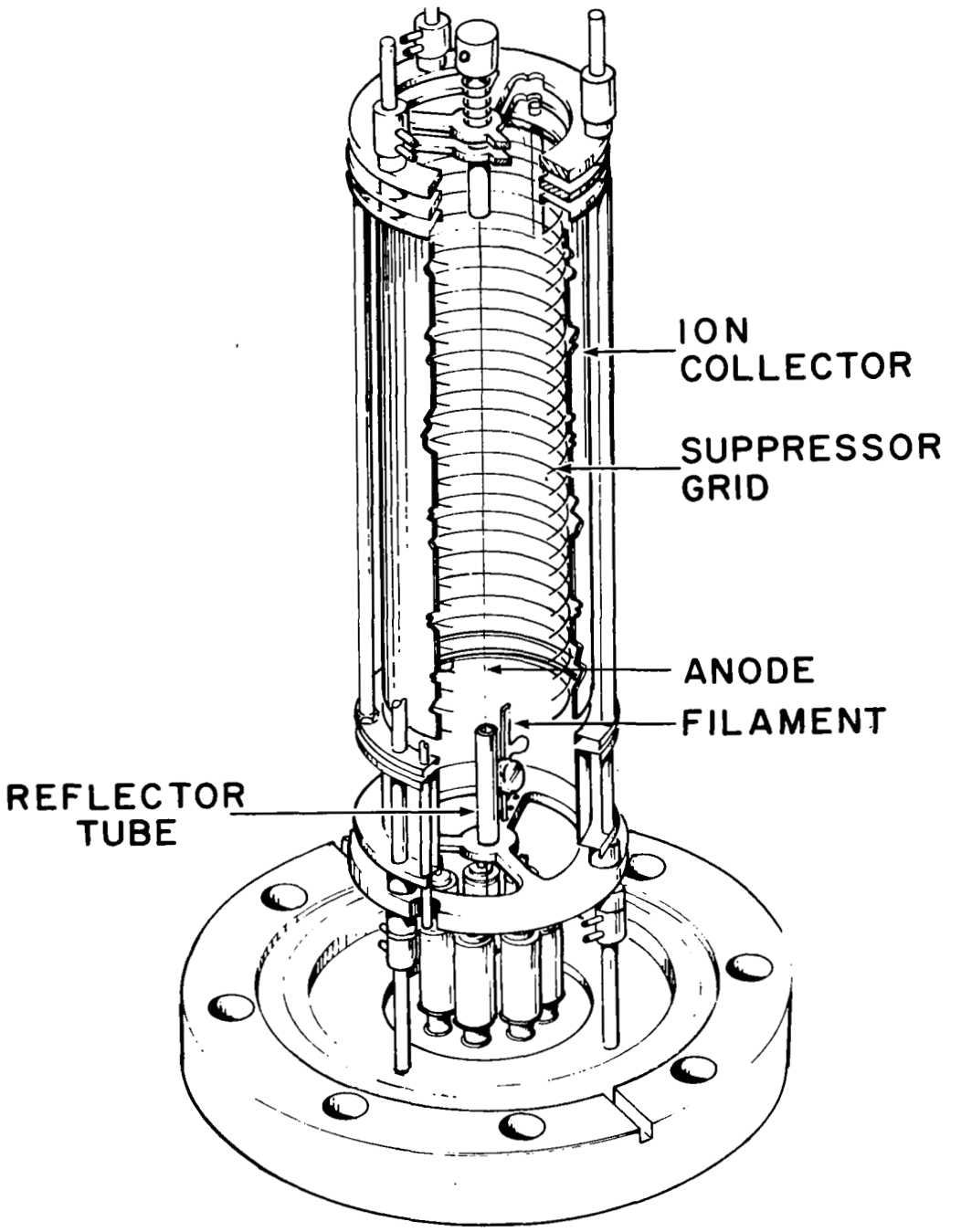

Figure 14 - Diagram of the Suppressor Grid Orbitron Gauge (SGOG). This gauge is identical to the Control Orbitron Gauge except for the suppressor-grid-ion-collector assembly. The electron orbiting volume is defined by the suppressor grid.

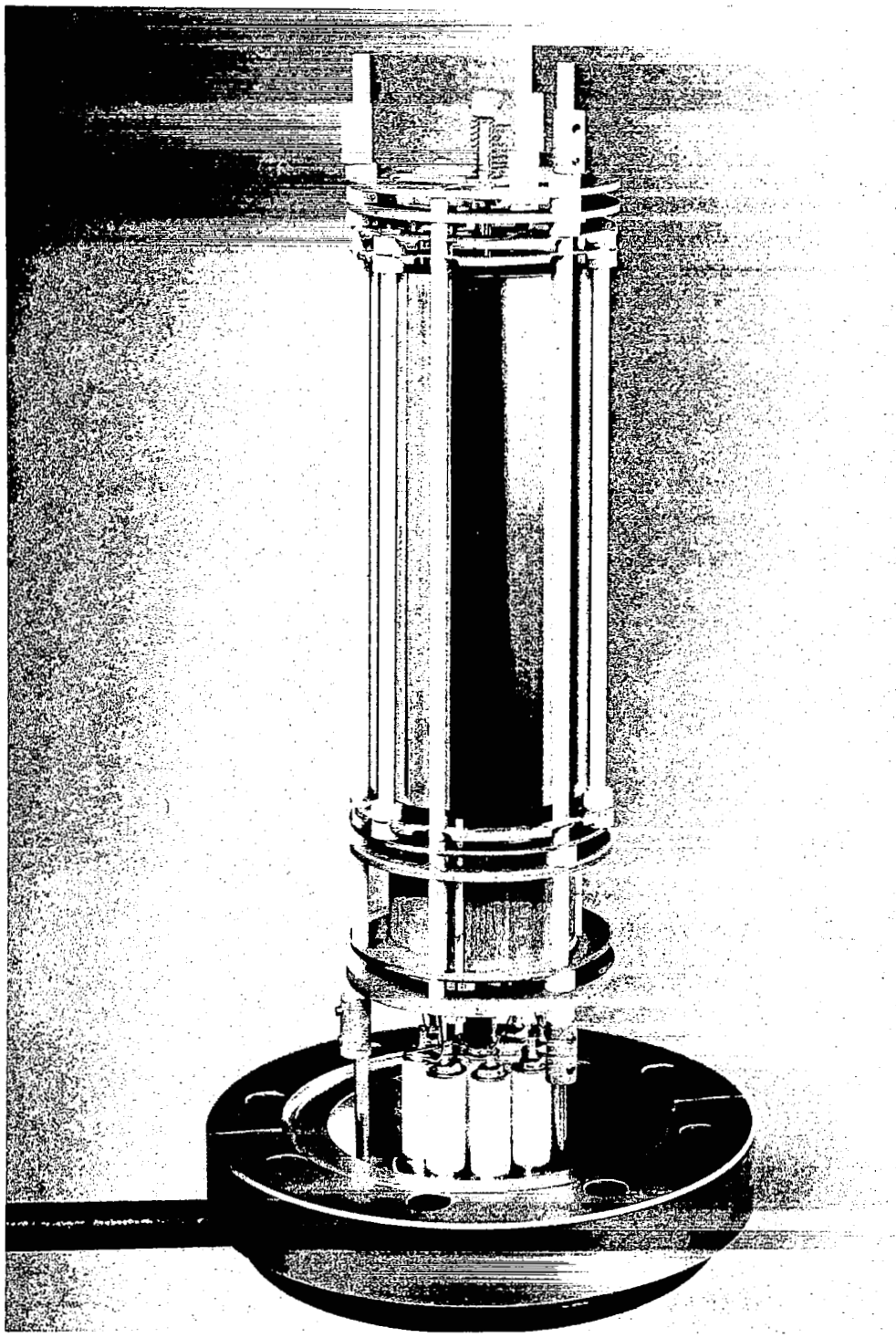

Figure 15 - Photograph of Suppressor Grid Orbitron Gauge

The lower cathode section and the suppressor grid have the same radius and therefore are held at the same potential in order to maintain a uniform field.

The ion collector in both gauges is connected to ground via an electrometer. The filament support assemblies are constructed such that the filament can be positioned at three radial positions within the gauge structures. These radial positions were 0.3R, 0.5R, and 0.7R from the anode, where R is the radius of the suppressor grid in the SGOG and R is the radius of the ion collector in the COG. The anode support system is designed so that various diameter anode wires can be used. In this study, two anode diameters have been used in the SGOG, 0.130 mm. diameter and 0.025 mm. diameter. High-temperature degassing of either anode was accomplished by Joule heating. A more detailed description of the orbitron gauges, as well as the fabrication techniques used in assembling them, has been presented previously.[3]

B. Effect of Anode Variation on Orbitron Response

The ion current to pressure response characteristics for an emission current of 3 μA, a filament position of 0.3R, and a tantalum anode of 0.130 mm. diameter are shown in Figure 16. A near-linear gauge response corresponding to a sensitivity of 0.054 A/torr has been observed.

In the 10^{-12} torr range, the response falls below the linear response line. An explanation of this effect can be found by examining Figure 17. In this figure the collector current has been plotted versus the suppressor grid voltage at a pressure which is less than 10^{-12} torr. At suppressor grid voltages between 0 and -12 V, a positive current was observed at the ion collector. However, beyond -12 V the current observed at the collector was negative. The positive current corresponds to photoelectrons leaving the collector, whereas the negative current indicates electrons which are arriving at the collector. We speculate that this latter effect results from photoelectrons from the suppressor grid being suppressed onto the collector. At -13 V, a negative signal is measured at the collector corresponding to approximately -5×10^{-14} A. If this negative background level is added to the data shown in Figure 16, the low-pressure data points are moved up to the linear gauge response line. A better choice for the suppressor grid potential, therefore, would be approximately -12 V.

Subsequently, a 0.025 mm. diameter tungsten anode was mounted in the suppressor grid gauge with the reflector tubes electrically isolated from all other components in the gauge.

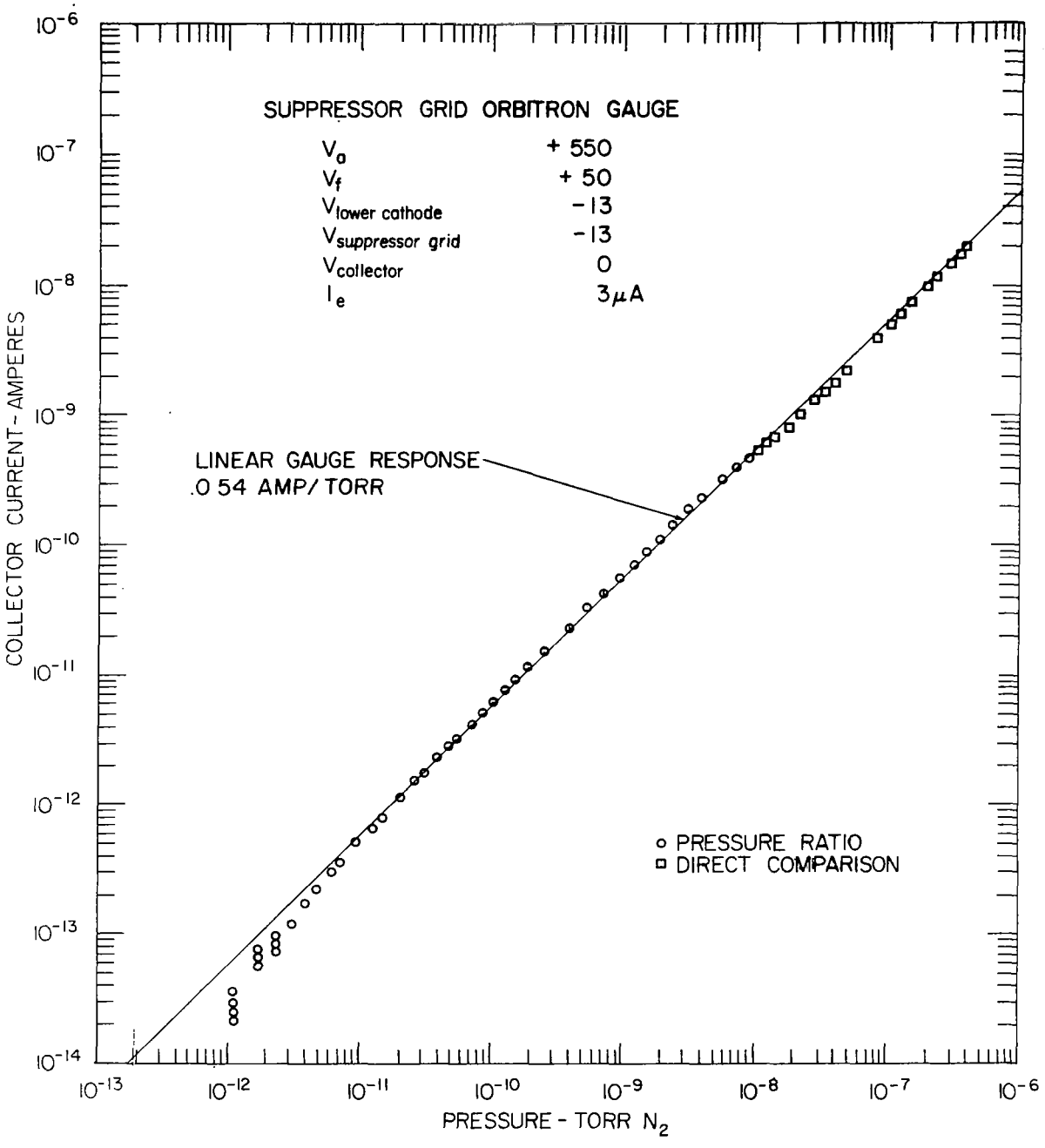

Figure 16 - Response Curve for the Suppressor Grid Orbitron Gauge. These data were collected for a 0.130 mm. diameter anode and a filament position of 0.3R.

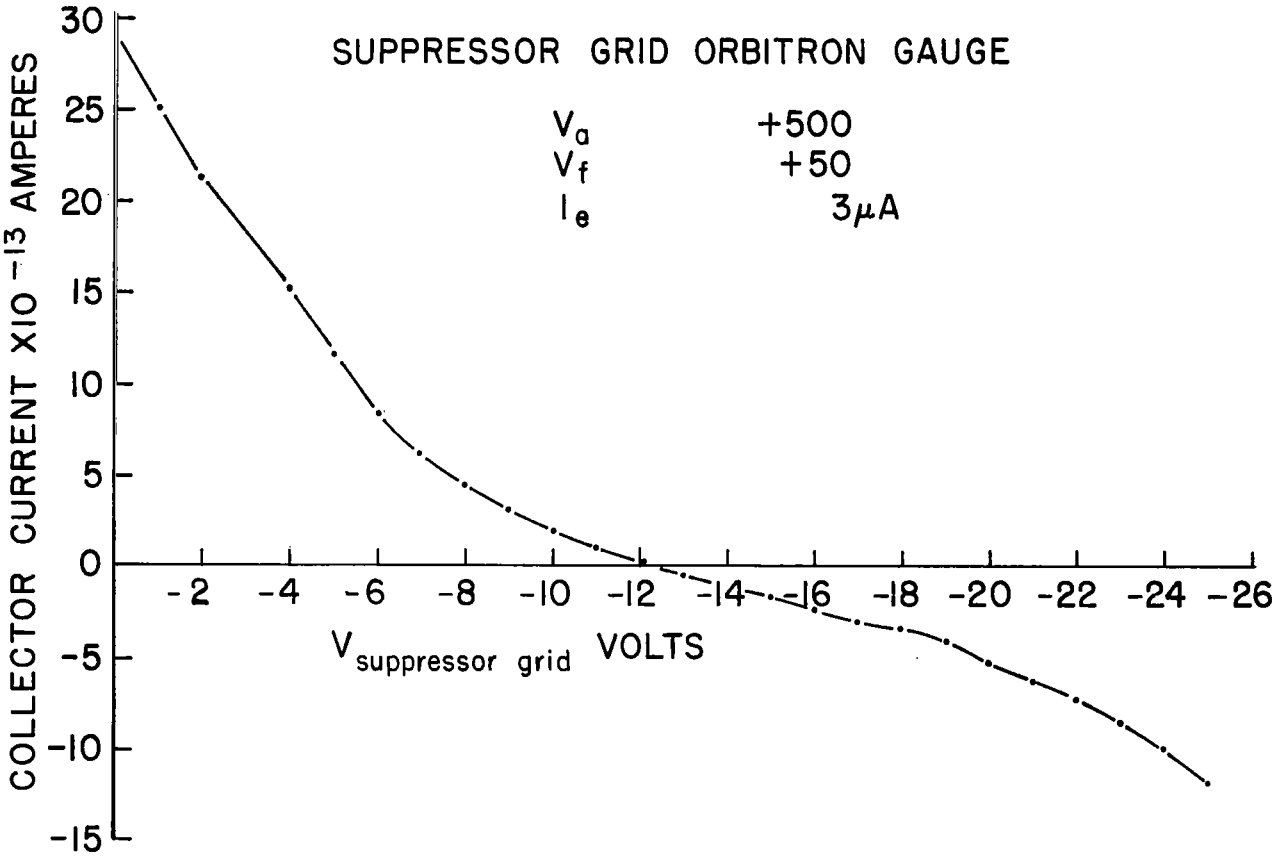

Figure 17 - Background Current Versus Suppressor Grid Voltage for an Anode Diameter of 0.130 mm. Negative currents can be generated at the ion collector by the collection of secondary emitted electrons from the suppressor grid.

An attempt was made to operate the gauge with the same operating voltage parameters as used in Figure 16. However, it was quickly determined that excessive filament current would be required in order to maintain a 3 μA emission level. Therefore, the filament potential was adjusted downward to 38 V. At this filament voltage level, the filament operation was near normal and a 3 μA current was established. Although extensive data were not collected in this condition, the sensitivity of the gauge appeared to be in the range of 0.034 A/torr; somewhat less than is shown in Figure 16.

The required change in filament potential indicates that changing the anode diameter caused a significant change in the field conditions. This change is to be expected because of the logarithmic nature of the field within the orbitron gauge. Therefore, the lower sensitivity may be explained by observing that the volume within the gauge in which orbiting electrons have enough energy to cause ionization has been reduced. In an effort to extend the path length of the orbiting electrons in order to compensate for this reduction in sensitivity, the reflector tube potentials were varied. It was determined that the maximum gauge response could be achieved while maintaining the reflector tubes at approximately -40 V. The effect of reducing the reflector tube potential is to improve the reflection of the electrons from the ends of the electron orbiting volume. The anode voltage was also varied in an attempt to increase the effective ionization volume within the gauge.

Before a set of parameters was selected, a residual current study was conducted on the gauge at a pressure less than 10^{-12} torr. This procedure was followed so as to insure the best possible low-pressure response characteristics. Figure 18 displays the current to the ion collector versus the suppressor grid potential for three anode voltages: 750 V, 650 V, and 550 V. These data were collected for a reflector tube potential of -40 V. A most striking feature of these data is their disagreement with the data presented in Figure 17; however, the effects of the suppressor grid are clear. At this point it is not clear why the suppressor grid potential is so much higher for the large diameter anode than for the small diameter anode.

In Figure 19, the collector current versus reflector tube potential is plotted for three anode voltages and for a total pressure less than 10^{-12} torr. The suppressor grid data shown in Figure 18 indicate that the high background currents which are shown at -40 V in Figure 19 present no serious problems. However, operation of the gauge in the ultrahigh vacuum range, with a reflector tube potential at -40 V, would not be desirable if the suppressor grid were not available to suppress the large background current which is present.

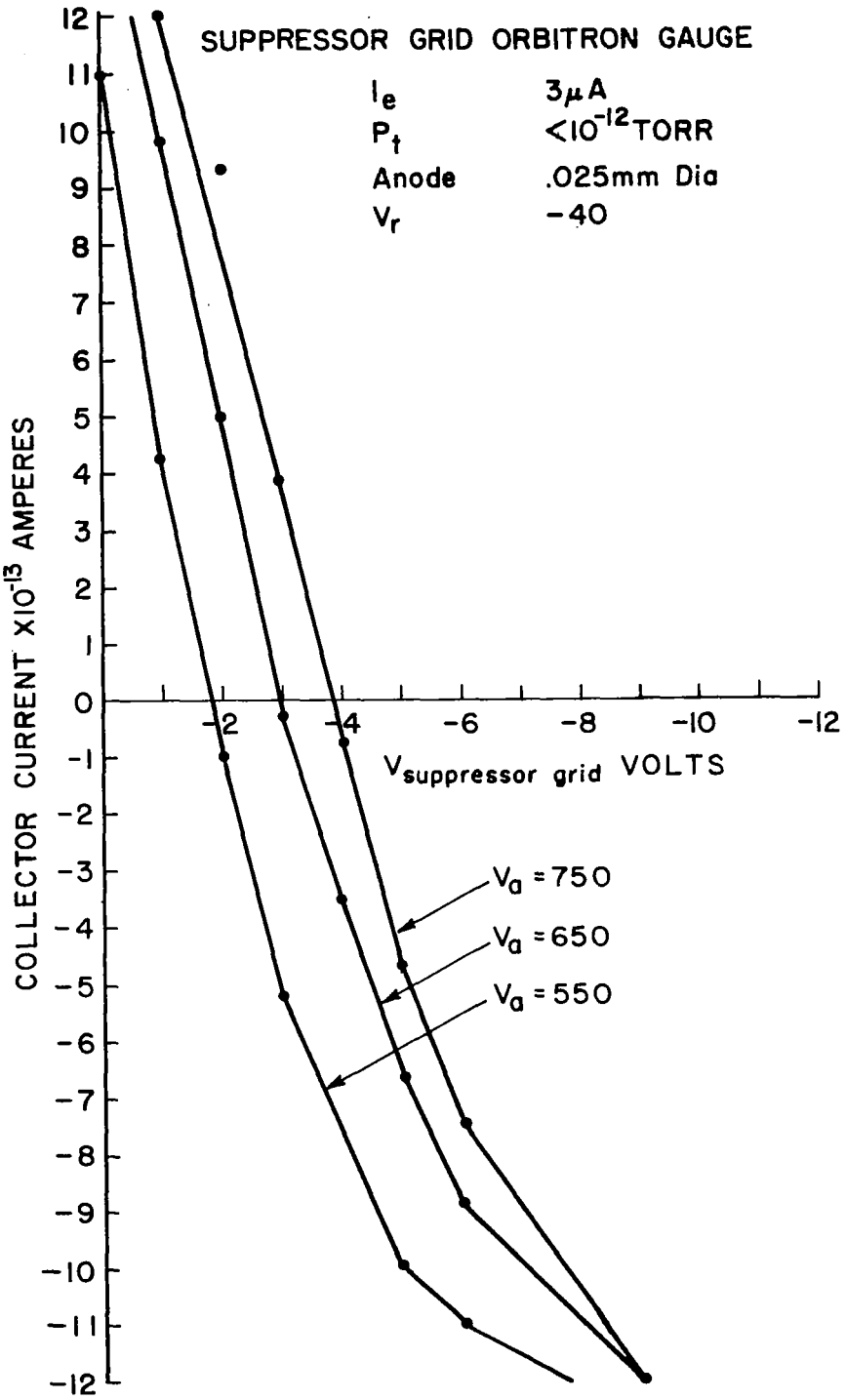

Figure 18 - Background Current Versus Suppressor Grid Voltage

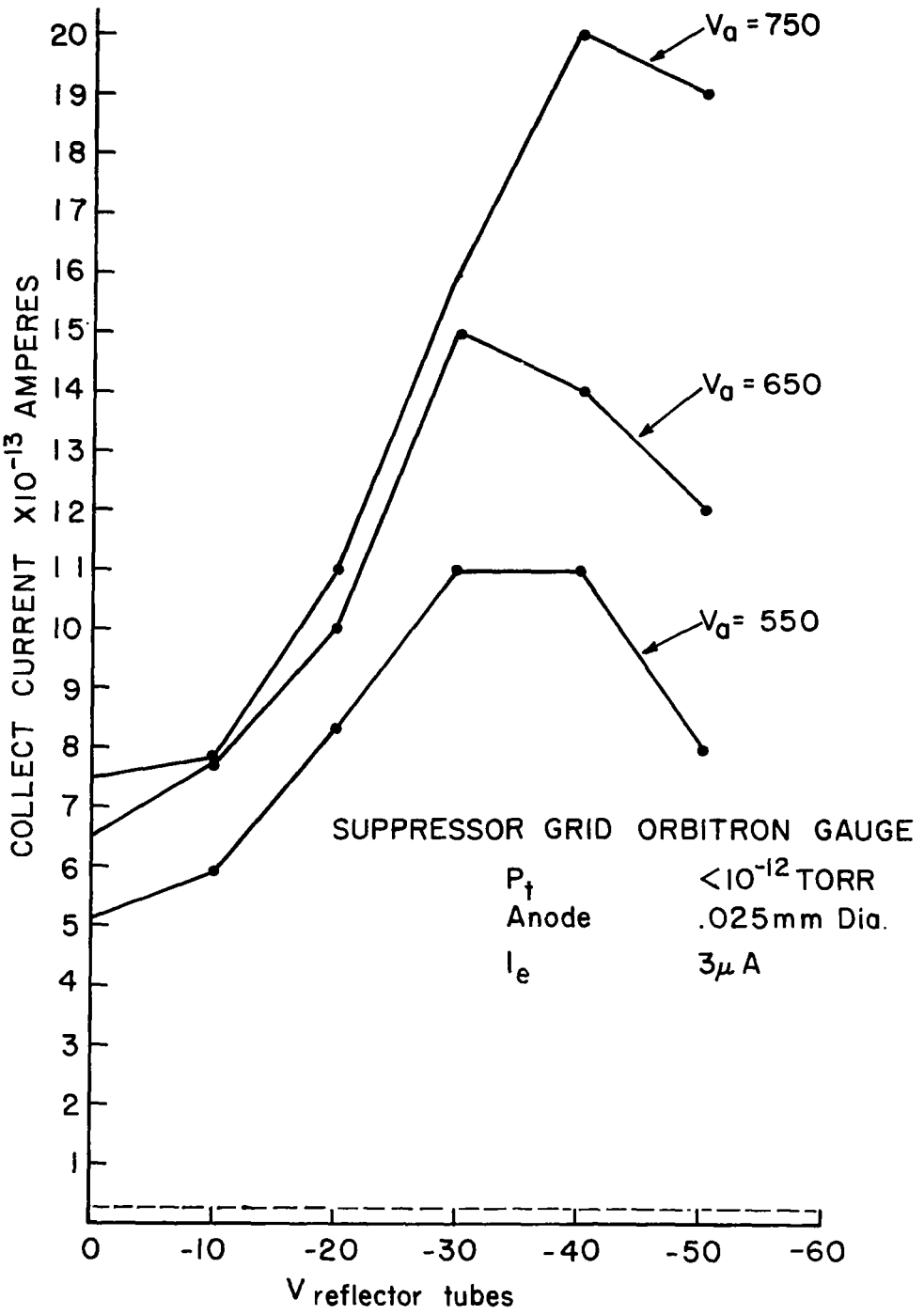

Figure 19 - Residual Collector Current Versus Reflector Tube Potentials. The effects of varying the reflector tube potential on the residual background current at the ion collector are shown for three anode potentials.

Figure 20 shows a pressure-to-collector current response curve for the suppressor grid orbitron gauge operating with an anode voltage of 750 V, a reflector tube potential of -40 V, and an emission current of 3.0 μA. The gauge response from 10^{-8} torr to 10^{-12} torr was approximately linear, corresponding to a gauge sensitivity of 0.10 A/torr. Above 10^{-8} torr, the gauge response became nonlinear and the sensitivity increased rather steeply. This increase in sensitivity may be due to the contribution of electrons which are coming from the ionization of the gas. Because of the negative reflector tube potential, it appears that the electrons are being contained in orbit more effectively, and thus the additional electrons due to ionization become an important consideration at pressures above 10^{-8} torr.

Although the nonlinear response characteristics above 10^{-8} torr were not the primary concern of this study, additional data have been collected. Figure 21 displays the gauge sensitivity versus filament voltage for selected pressure levels above 10^{-8} torr. These data were collected with the suppressor grid orbitron gauge, using a 0.025-mm. diameter tungsten anode, a reflector true potential of -40 V, and an anode potential of +750 V. An attempt to explain this nonlinear behavior has been made and is included as an appendix to this report (Appendix A).

C. Effect of Filament Position on Orbitron Response

A filament position study has been conducted on the control orbitron gauge. Figure 22 summarizes the data which have been collected in terms of the gauge sensitivity versus pressure. The three curves shown correspond to the three filament positions, 0.3R, 0.5R, and 0.7R. The filament potential in each case has been adjusted so as to achieve maximum sensitivity for an operating anode voltage of 553 V. The anode voltage was selected so that the data could be compared with previously collected data on this gauge.

The data in Figure 22 indicate that the sensitivity of gauge changes by almost an order of magnitude between each of the respective positions. Also, the sensitivity fails to attain a fixed value for the 0.7R and 0.5R position data, whereas for the 0.3R position, less sensitivity variation is noticed. These data indicate that fewer electrons are going into stable orbits from 0.7R and 0.5R positions than from the 0.3R position. Therefore, empirically, one would expect that filament positions close to the anode would produce longer mean path length electrons than filament positions far from the anode.

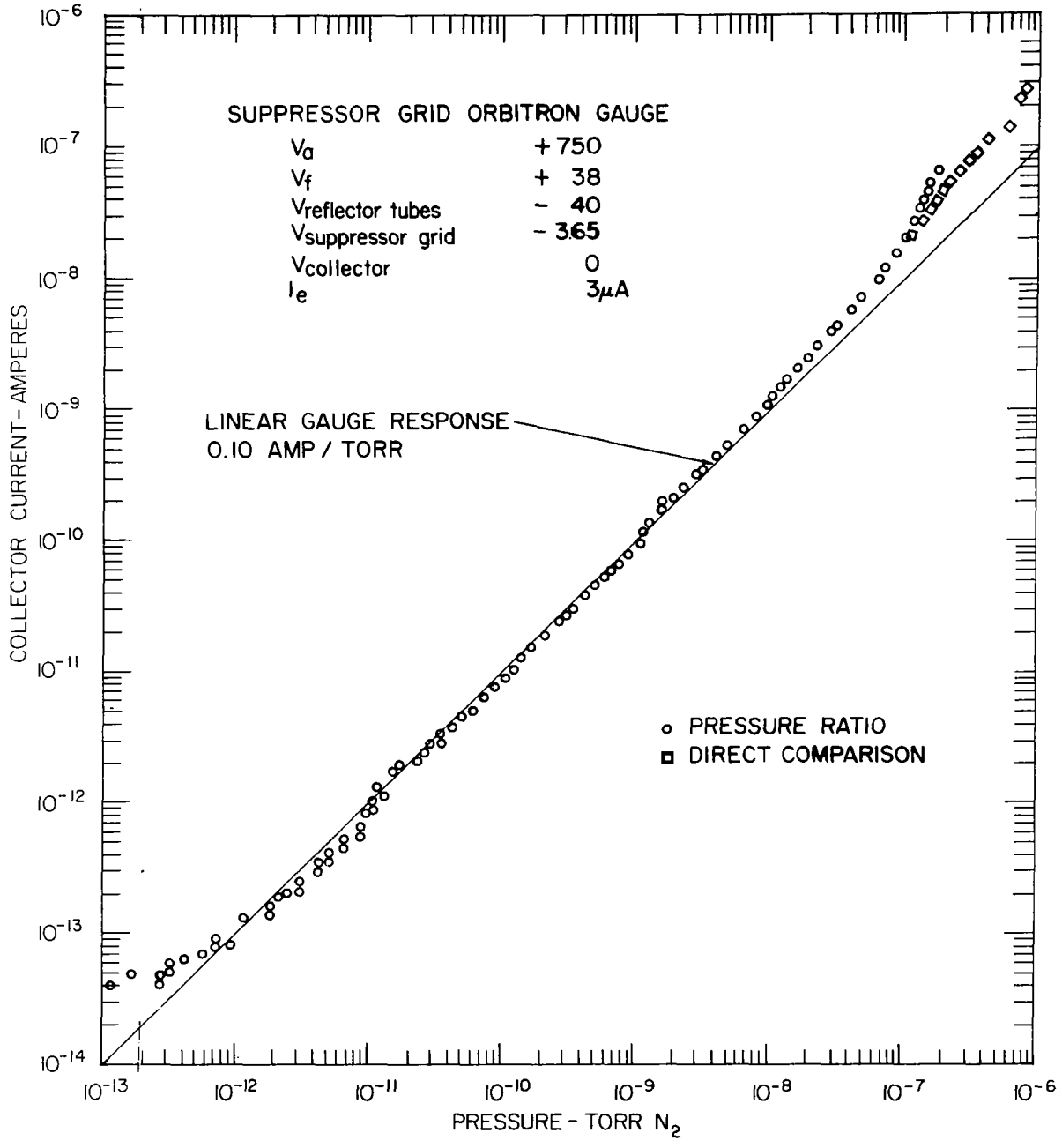

Figure 20 - Ion Collector Current Versus Pressure for the Suppressor Grid Gauge Using a 0.025 mm. Diameter Anode. These data indicate that the orbitron gauge is less linear using the smaller diameter anode. However, improved sensitivity has been achieved over the 0.130 mm. diameter anode.

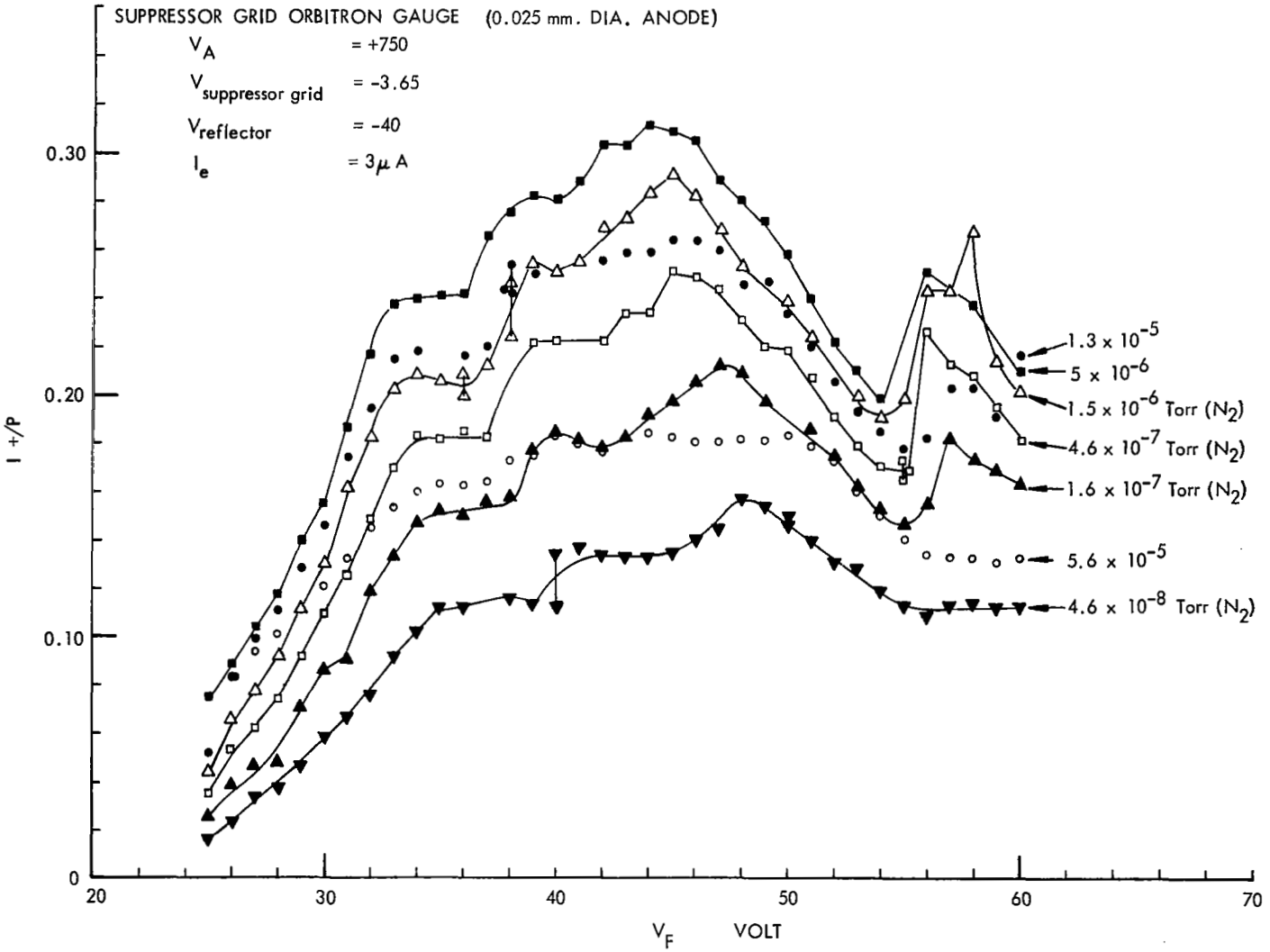

Figure 21 - Suppressor Grid Orbitron Gauge Sensitivity Versus Filament Voltage for 0.025 mm. Diameter Anode. Seven sets of data are presented, corresponding to seven different pressure levels.

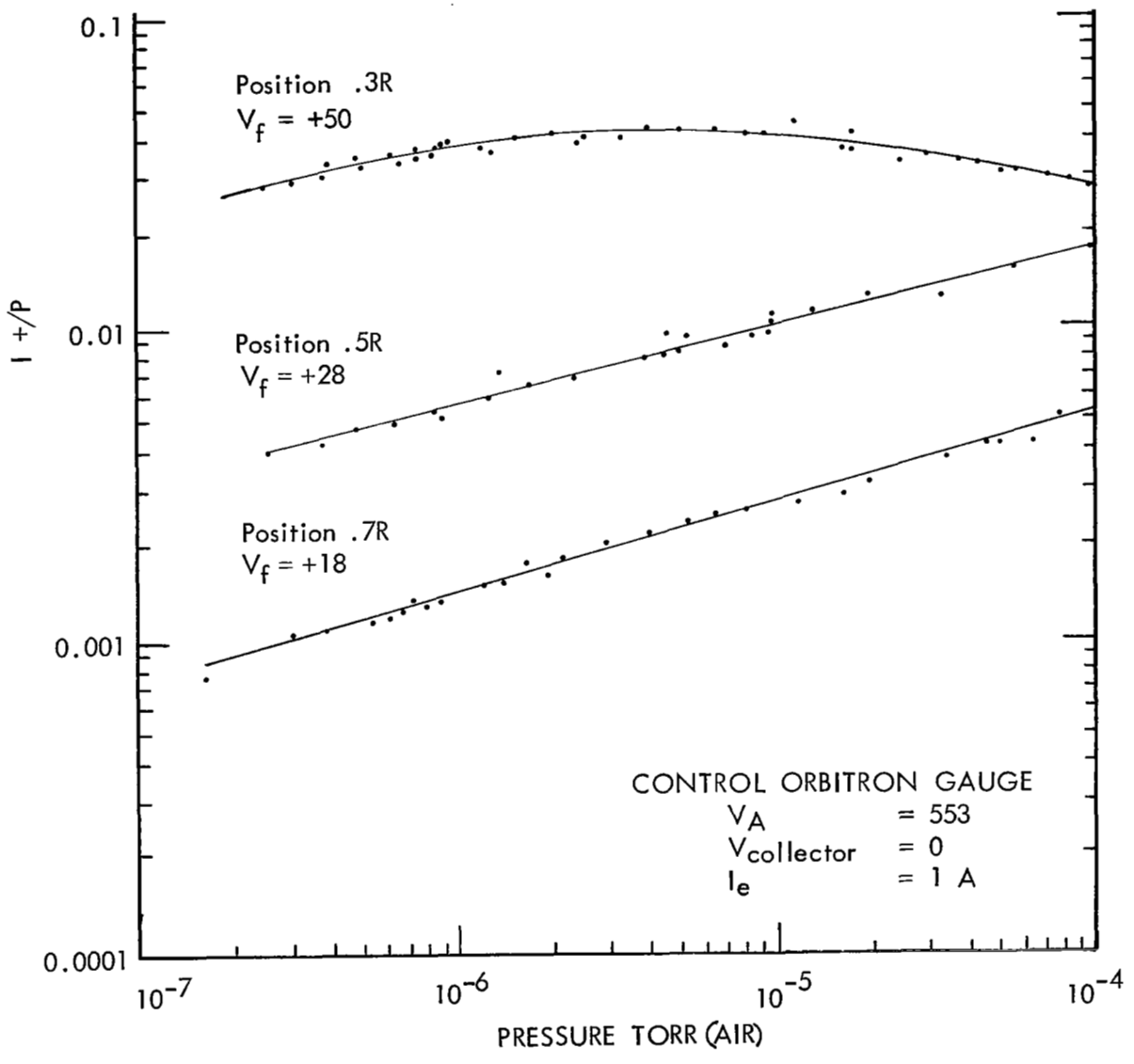

Figure 22 - Sensitivity of Control Orbitron Gauge Versus Pressure for Three Filament Positions. The filament potential was adjusted for each condition so as to maximize the gauge sensitivity.

D. Discussion

The use of the small-diameter anode wires (0.025 mm. diameter) did not have a serious effect on the stability of the gauge. It did produce higher gauge sensitivities, which imply that the electrons have longer mean free paths. The nonlinearity effect at higher pressures was noted at pressures corresponding to 10^{-8} torr and above. However, at the low-pressure end, the sensitivity of the gauge using the 0.045 mm. diameter anode appeared to be almost linear at a value corresponding to 0.10 A/torr. With this sensitivity, and with the capability to suppress the background current, the gauge is useful through the 10^{-12} torr range. Below that level, the adjustment of the suppressor grid voltage is very critical, and it may not be practical to attempt to extend the useful range of the gauge below 10^{-12} torr.

At this time there is little evidence which can explain the large difference between the data given in Figure 17 and Figure 18, or to relate the anode diameter, reflector tube potential, and suppressor grid potential. A speculative argument can be put forth: the electrons preferentially strike at a different position along the anode when the electron path lengths are extended. Photon production would be nonuniform along the anode and fraction of phqtons that the ion collector intercepts will be a function of path length. Additional data are needed to prove or disprove this hypothesis.

IV. DEVELOPMENT OF SMALL ORBITRON GAUGE

This section describes the design and fabrication of a small, glass-encased model of the orbitron gauge. The small unit employs the suppressor grid technique. The response characteristics of this gauge, hereafter referred to as the small orbitron gauge No. 1 (SOG No. 1), have been determined in the pressure range between 10^{-12} and 10^{-6} torr.

A. Design of Small Orbitron Gauge

The SOG No. 1 is shown schematically in Figure 23. The design of the gauge is based on the suppressor grid orbitron gauge design[3] which was developed on a previous NASA contract (NAS1-7458) and discussed in Section III.

The SOG No. 1 consists of three concentric electrodes and a hot filament electron source. The center electrode (anode) is a 0.13 mm. diameter

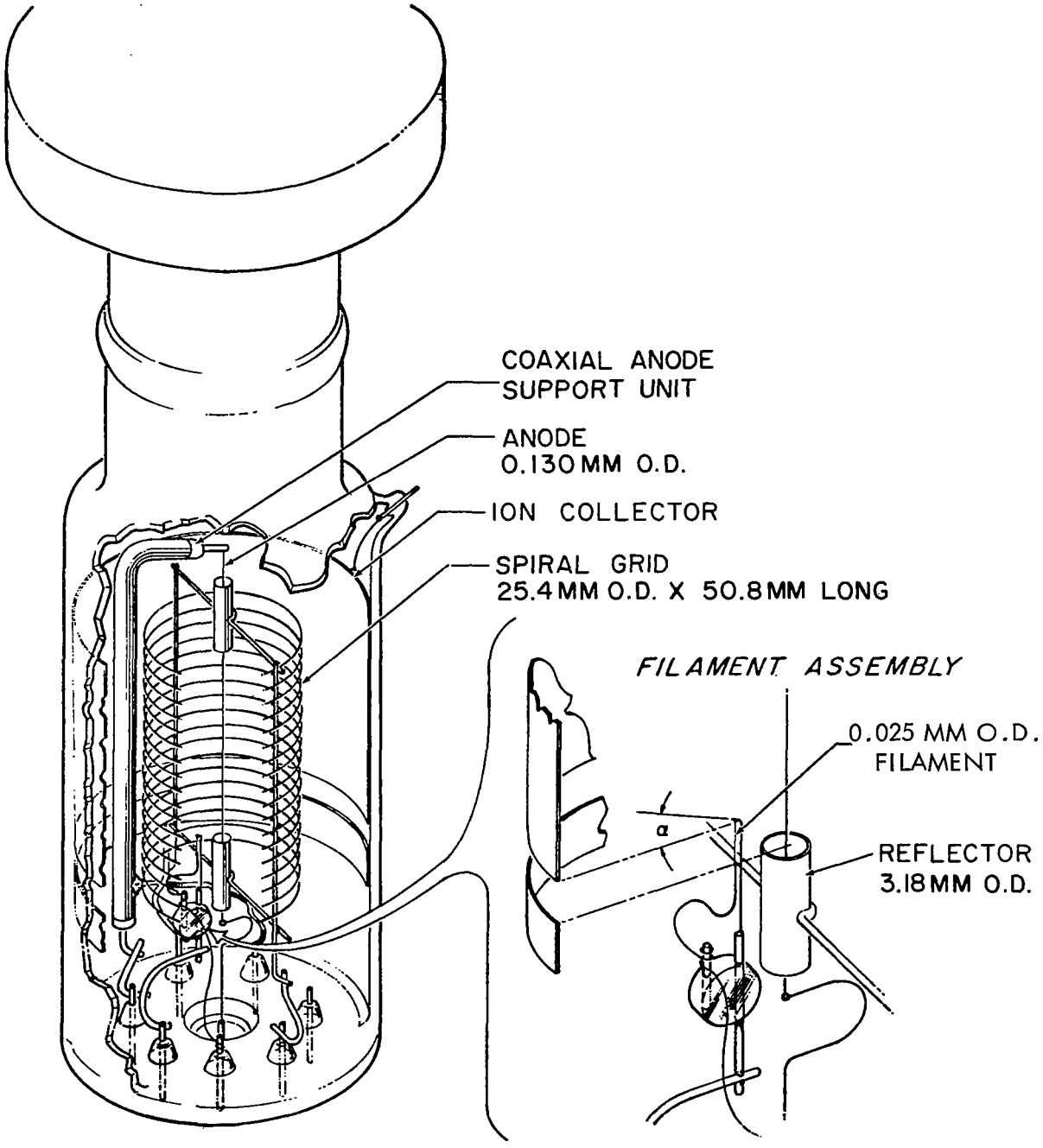

Figure 23 - Small Orbitron Gauge. Ions are generated by orbiting electrons within the spiral grid and are collected at the metal film ion collector deposited on the glass envelope of the gauge. The angle α in the filament assembly is $\sim 45°$.

tungsten wire, and is attached to the center pin of the pin base via a U-shaped spring and to a coaxial anode support unit. The coaxial support consists of a glass-encased metal support rod structure mounted from the pin base. A conducting metal film has been added to the outer surface of encasing glass tubes and is electrically connected to one of the pins in the pin base. By controlling the electric potential of the film, field perturbations resulting from the nonsymmetric position of the anode support rod in the gauge can be eliminated.

The second concentric electrode encloses the electron orbiting volume and consists of an open-ended grid structure (2.54 cm. O.D. x 5.1 cm. long) which is supported from the pin base. At each end of the grid, a 3.18 mm. O.D. x 12.7 mm. in. long stainless steel tube (0.25 mm. wall thickness) is mounted via a support rod which is attached to the grid supports. The 0.13 mm. in. tungsten wire described above passes through the center of the 3.18 mm. O.D. tubes.

The third electrode is a platinum coating on the inside surface of the glass envelope. This coating is divided into two electrically isolated sections, the larger of which is used to measure ion current. The smaller section is used to provide a guard ring between the pin base and the ion collector, and to assure the maintenance of symmetric field conditions within the electron orbiting volume. The two coated sections are separated by a 4.8 mm. gap. The location of the gap with respect to the 3.18 mm. O.D. tubes discussed above is shown in Figure 23.

The hot filament electron source is a 0.025 mm. x 3.18 mm. long tungsten wire, which is mounted within the electron orbiting volume via a filament support assembly. The dimensions of the filament and support unit are given in Figure 23. The main support of the filament unit is located at approximately 1.6 mm. from the anode wire. The filament is positioned on a line passing through the main support and making an angle (α) of $\sim 45°$ with a radial line passing through the main support.

B. Response of Small Orbitron Gauge

The ion current versus pressure response data are shown in Figure 24. In the low-pressure region, a positive background current was measured at the ion collector, which corresponded to 5.6×10^{-12} A. The operating parameters were varied in an attempt to eliminate this positive pressure independent current. It was determined that this current was a function of the filament heating current. This fact suggests that the positive background current was due to a positive ion current which was being generated from the hot filament surface.

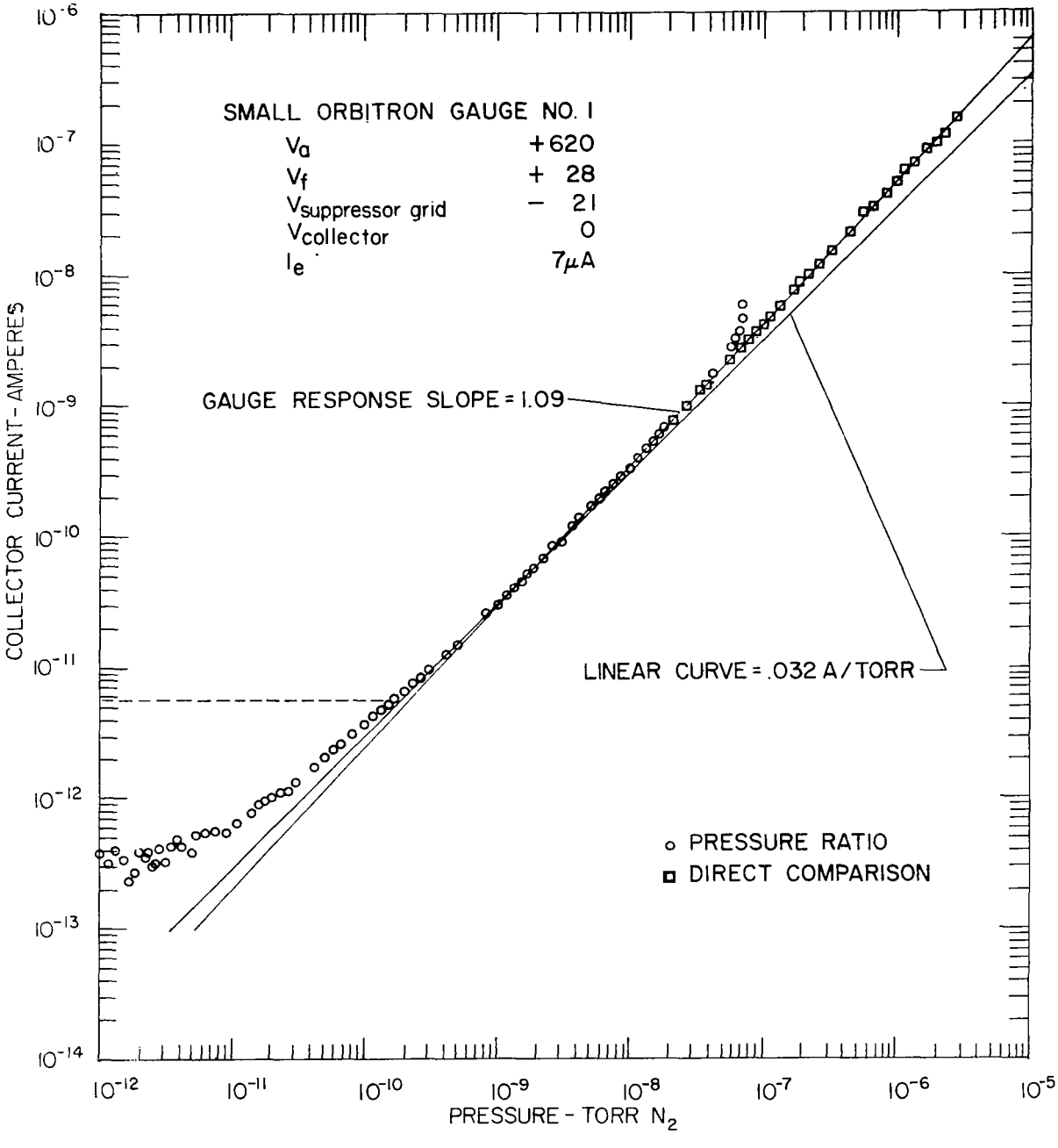

Figure 24 - Ion Collector Current Versus Pressure for the SOG No. 1. A positive background current of 5.6×10^{-12} A has been electronically suppressed at the electrometer for the collection of these data. The gauge displayed an approximately linear response between 4×10^{-10} and 4×10^{-9} torr corresponding to a sensitivity of 0.032 A/torr.

An evaluation of the low-pressure response characteristics of the SOG No. 1 was conducted by supplying a zero suppression signal, equal to 5.6×10^{-12} A, to the ion collector electrometer. The dashed line in Figure 24 indicates the level of zero suppression. The response data below 10^{-11} torr are too scattered to be of any practical value. Above 10^{-11} torr, the gauge response was nonlinear. The data fell along a line with a slope of 1.09. A linear line has been drawn into the figure, corresponding to a sensitivity of 0.032 A/torr. This line could be used to describe the gauge response characteristics between 3×10^{-9} and 3×10^{-10} torr.

The discontinuity in the pressure ratio data at approximately 5×10^{-8} torr corresponded to the breakdown of the pressure ratio system mentioned earlier.

C. Discussion

The response of the small orbitron gauge indicates that its primary usefulness lies in the pressure range between 10^{-11} and 10^{-6} torr. Although the response in this range is not linear, it can be calibrated. The major reasons for employing a small orbitron gauge were as follows: (1) the size is approximately equivalent to a Bayard-Alpert gauge, and (2) because the filament dimensions and power requirements are small, the filament has a small interaction with the environment which is being measured. The positive ion background current could be eliminated from future small orbitron gauges by design modifications. However, unless the sensitivity of the gauge in the low-pressure region is significantly increased by a factor of at least 3 or 4, it does not appear that this gauge would be useful below 10^{-11} torr.

V. TECHNIQUES FOR GAUGE TESTING AT LOW PRESSURES THROUGH USE OF EXISTING TECHNOLOGY

Vacuum technology may be divided into two major areas of interest: (1) the production of evacuated environments, and (2) the measurement of the level of evacuation which exists therein. The technology of evacuation has been advanced to the point where space simulation is a probable reality. It is because of the lack of available low-pressure standards that a more precise statement of space simulation capabilities is not made. This situation is, of course, understandable, since space simulation at present is a science which functions at the limits of the art of vacuum technology. However, because of recent advancements in both total and partial pressure monitoring devices[9-12] it is becoming feasibile to expect a firmer base for space simulation measurements.

The increased confidence resulting from the use of improved monitoring devices will come only with an adequate understanding of their response characteristic in the low pressure realm and a correlation of their response to already accepted standards, i.e., adequate calibration. Although some calibration tests have been conducted at low pressures ($< 10^{-10}$)[13-20] these measurements have not been directly related to absolute and/or accepted standards.

In the following sections we have discussed the basic problem of low pressure standards and two techniques for gauge testing. The gauge testing techniques permit the development of low pressures which have calculable value and which can be used for comparison of gauges.

A. The Basic Problem

The basic problem associated with the production of extreme low pressure environments ($< 10^{-12}$ torr) and the establishment of measurable relationships between that pressure level and an accepted standard is primarily one of pumping capacity. Extreme low pressure environments are usually established by means of very high speed capture pumping such as is achieved by LHe temperature cryopanels. This type of pumping performs well at low pressure; however, because of its limited* gas handling capacity the pump surfaces saturate rapidly at higher pressure levels. It is in this higher pressure range ($> 10^{-5}$ torr) where accepted pressure standards are available. However, the state of the art of vacuum technique is such that this type of problem can be circumvented by the series application of two well known calibration techniques, viz., the pressure ratio technique[21] and the pressure reference transfer technique.[22]

B. Pressure Ratio Technique

The pressure ratio technique as it is normally used is outlined schematically in Figure 25. An equilibrium flow of a test gas is established from a reference volume (Vol. 2) through a restricted conductance (C') into a test volume (Vol. 1) which is evacuated by a conductance limited UHV pumping station. The pressure (P_1) at the test gauge is determined by the equation:

$$P_1 = \frac{Q(C_1+S_1)}{C_1 S_1}$$

* The capacity of a cryopump to handle large quantities of gas is quite limited when compared to a diffusion pump. However, to obtain the high pumping speed of a nonfilled LHe cooled surface with diffusion pumps is not feasible.

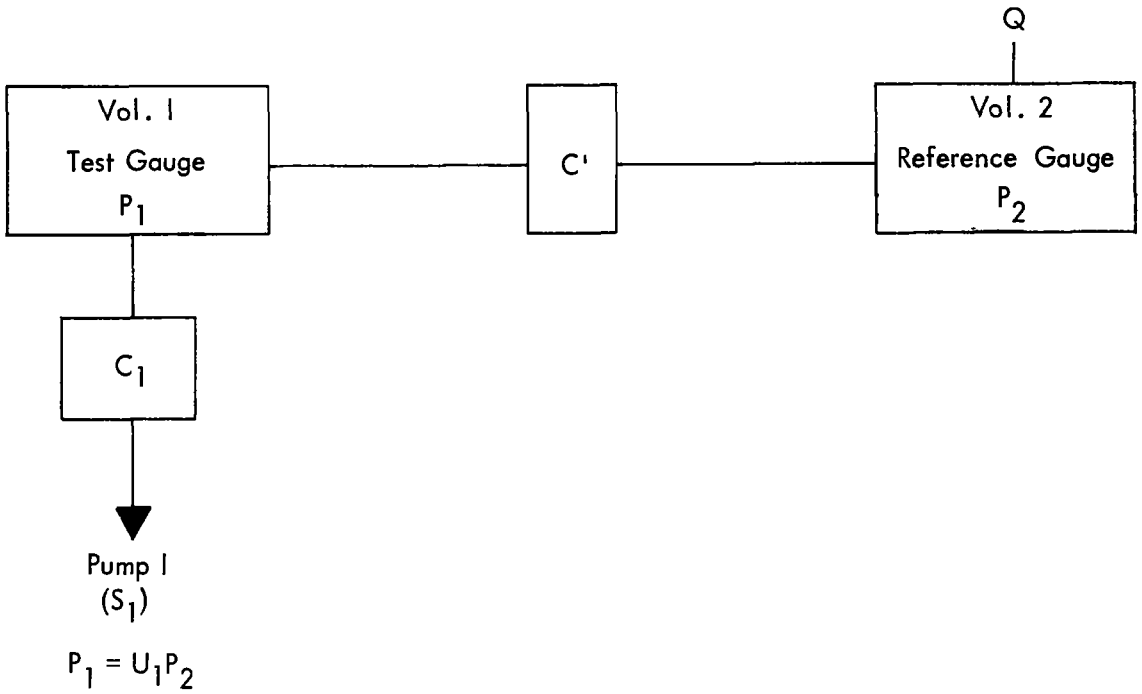

Figure 25 - Diagram of Pressure Ratio Technique. The flow (Q) of a test gas through the conductance (C') establishes a pressure ratio between the reference gauge and test gauge positions. This relationship can be used to determine the pressure in the test volume (P_1) by measurements of pressure in the reference volume (P_2) as long as (1) P_1 is controlled by equilibrium flow conditions; (2) C' remains constant; and (3) the pumping speed for the test gas from Vol. 1 remains constant.

where Q = a steady flow of a test gas through the pressure ratio system,

C_1 = conductance limiting the UHV pump, and

S_1 = pumping speed of the UHV system for the test gas.

The pressure (P_2) at the reference gauge is

$$P_2 = \frac{Q(C_1S_1+C'S_1+C_1C')}{C_1S_1C'}$$

where C' = conductance between test gauge position and reference gauge position. The pressure ratio between the test and reference gauge positions is given by

$$\frac{P_1}{P_2} = \frac{C'(C_1+S_1)}{C_1S_1 + C'S_1 + C_1C'} = U_1$$

If C', C_1 and S_1 are constant, then U_1 is constant and

$$P_1 = U_1P_2$$

Therefore, the pressure at the test gauge position can be determined by measuring the pressure at the reference gauge position, if the following requirements are maintained: (1) a steady flow of a test gas is established, (2) the conductance between the upstream (reference) position and downstream (test) position does not change, and (3) a constant pumping speed for the test gas is maintained by the conductance limited pumping station. Implied in this technique are the requirements that the background pressure is small compared with the flow regulated pressure P_1 and that there are no other sources or sinks for the test gas between the reference gauge and test gauge positions. However, this requirement does not preclude pumping on the reference volume.

A modified pressure ratio technique is outlined schematically in Figure 26. In this case a conductance limited pump (2) has been connected to the reference chamber (Vol. 2). The equations governing the pressure relationships in this system are also presented. Again the pressure ratio can be written as a constant if C', C_1 and S_1 are constant, i.e.,

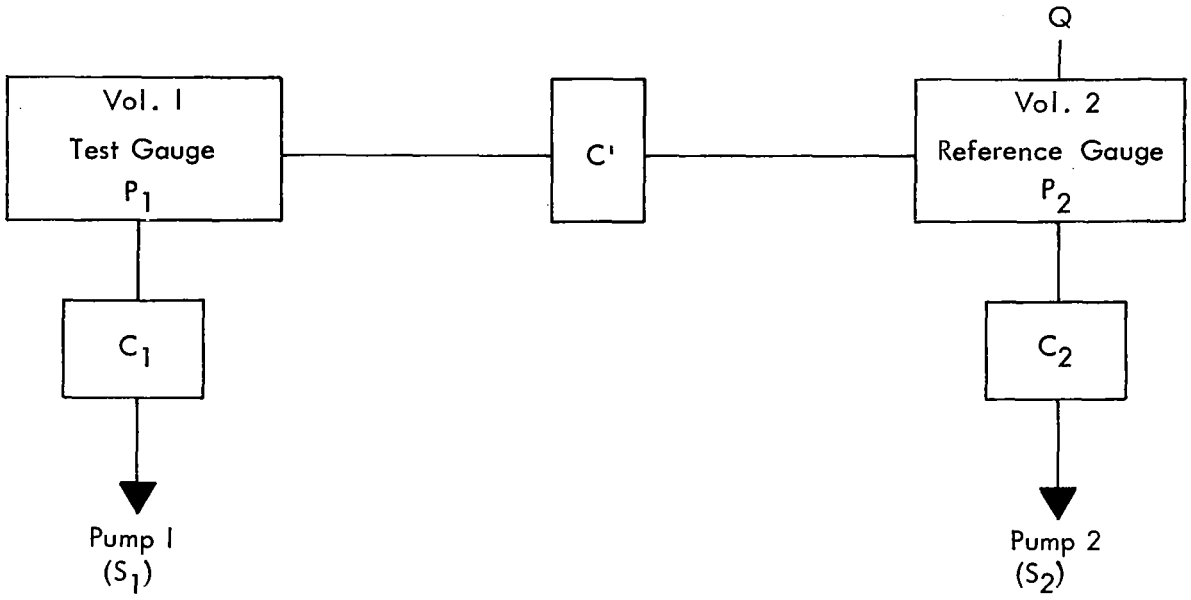

$$P_2 = \frac{Q}{S}$$

$$S = \frac{C_2 S_2}{C_2+S_2} + \frac{C'C_1S_1}{C_1S_1+C'S_1+C_1C'}$$

Q = Rate of gas flow into Vol. 2

Q_1 = Rate of gas flow from Vol. 2 via Pump 1

Q_2 = Rate of gas flow from Vol. 2 via Pump 2

$$Q = P_2 S = Q_1+Q_2$$

$$Q_1 = P_2 \frac{C'C_1S_1}{C_1S_1+C'S_1+C_1C'}$$

$$P_1 = \frac{\frac{Q_1}{C_1S_1}}{\frac{}{C_1+S_1}} = P_2 \frac{C'(C_1+S_1)}{C_1S_1+C'S_1+C_1C'}$$

Figure 26 - Diagram of a Modified Pressure Ratio Technique. The flow of test gas into the reference volume is pumped by pump 2 via C_2 and by pump 1 via C' and C_1 . The ratio U_1 is determined by C' , C_1 and S_1 only.

$$\frac{P_1}{P_2} = \frac{C'(C_1+S_1)}{C_1S_1 + C'S_1 + C_1C'} = U_1$$

Therefore, again we can write

$$P_1 = U_1P_2$$

Once U_1 is determined and can be established as a constant the accuracy with which P_1 is determined is a function of the accuracy of the measurement of P_2 for a given calibration test. If P_2 can be related to an accepted standard, P_1 can be related to the same standard through U_1 .

The advantage of the modified pressure ratio technique can now be easily seen by noting that the pressure in Vol. 2 can be achieved by high capacity pumping techniques and, therefore, can be related to accepted standards without experiencing the pumping capacity limitations which would result by attempting to operate Pump 1 in the high pressure ranges.

The pressure P_2 in Vol. 2 can be related to accepted pressure standards via the pressure reference transfer technique.[22] Figure 27 outlines schematically a combination pressure ratio and pressure reference transfer technique.

C. Pressure Reference-Transfer Technique

The pressure reference-transfer technique is displayed schematically in the right-hand side of Figure 27. The pressure reference transfer cycle begins after an ultimate pressure has been obtained in Vol. 2 with no flow of test gas, i.e., $Q = 0$. The reference transfer gauge (RTG)* is valved into Vol. 3 and a desired flow of test gas is then established. Once a stable condition has been reached the output signal (ion current) from the RTG is measured. Then the RTG is isolated from Vol. 3 and valved into Vol. 2. The flow of test gas, Q , is increased until the ion current from the RTG reaches the previously measured output which was observed when the RTG was monitoring Vol. 3. Because of the symmetry of the system the pressure of the test gas in Vol. 2 (P_2) is identical to the pressure previously monitored in Vol. 3. In effect a given (yet unknown) pressure of a test gas has been transferred from Vol. 3 to Vol. 2. The pressure of the test gas in Vol. 3 (P_3) following the above cycle is now higher than the Vol. 2 since Q was increased during the cycle. The pressures P_2 and P_3 are related by the equation

---

* No requirement is placed on the accuracy of this gauge. It is used only to determine similar environmental conditions.

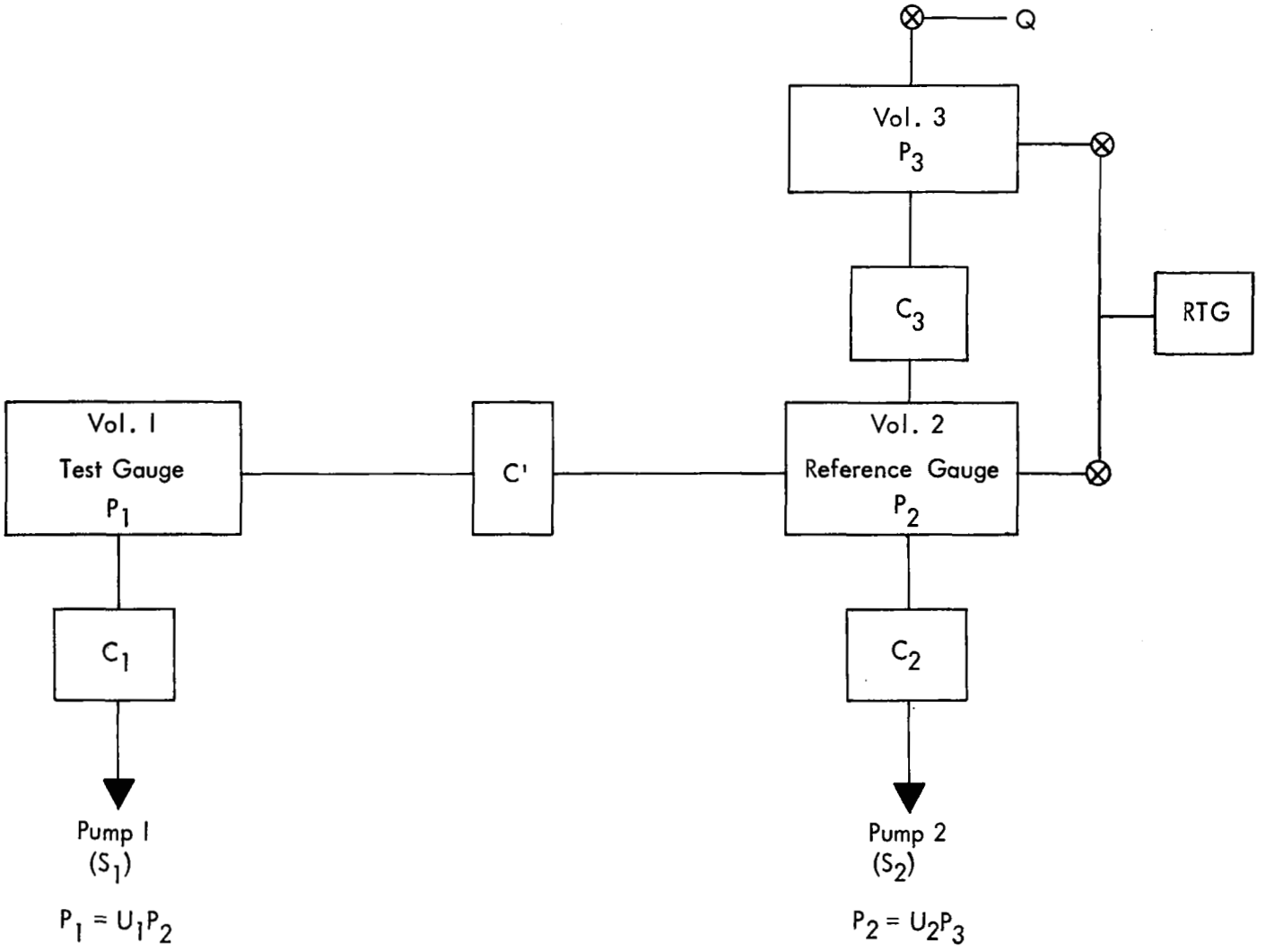

Figure 27 - Diagram of a Series Combination of Pressure Ratio Technique and a Pressure Reference Transfer Technique. The Reference Transfer Gauge (RTG) is alternately valved into Vol. 3 and Vol. 2 and the flow of test gas Q is sequentially adjusted to perform the pressure reference cycle.

$$P_2 = U_2 P_3$$

where U_2 = constant if S_2 , C_2 , C' , C_1 and S_1 are constant.* Now by isolating RTG from Vol. 2 and valving it into Vol. 3 another cycle can be performed. In fact, iteration of this cycle can be performed until P_3 is at a level which can be reliably measured. Then by simple calculations the pressure $P_2(n)$ at the n^{th} cycle can be determined by the equation

$$P_2(n) = U^{r-n} P_3(r)$$

where r is the cycle at which the reference pressure was determined.

With a value for U_2 of approximately 0.1 a fixed calibration point can be obtained in each decade per run. However, when the pressure reference technique is used as a reference for the pressure ratio technique a run can be made considerably slower so as to permit recording detailed response characteristics for a test gauge in Vol. 1 with stops at the accurately determined calibration points (one per decade per run).

If the value of $U_1 \sim 10^{-3}$ and a background level of $\sim 10^{-11}$ torr can be maintained in Vol. 2, then with appropriate background correction to the P_2 value, calibrations in the 10^{-14} torr range can be achieved.

D. Discussion

Both total pressure and partial pressure devices can be calibrated in the above described manner. However, with partial pressure devices background correction will be much simpler and less restrictive.

The prime requirement for the pressure ratio system is that the pressure in the test volume (Vol. 1) be established by the flow conditions and therefore the background pressure must be significantly below the pressure level to be calibrated. Because reliable response characteristic data for presently available pressure transducers in the range below 10^{-12} torr are lacking, it is uncertain how to determine when such a background situation exists. The alternative is to employ extreme vacuum techniques to evacuate Vol. 1, such as those employed for the work reported in Sections II, III, and IV.

---

* In practice $C' \ll C_1$ and therefore the pumping effect due to S_1 via C_1 and C' could usually be omitted.

VI. CONCLUSIONS

The following conclusions can be drawn from the material presented in this report.

1. The design of the experimental buried collector gauge (EBCG) does permit effective degassing of the lower grid end (shield) electrode.

2. The background currents to the ion collector in a well degassed EBCG are sufficiently stable to permit dependable measurements down to the low 10^{-13} torr range.

3. The EBCG filament design, type, and placement are critical to the gauge constant. Additional work is needed to rigorously define the filament parameters.

4. The operating parameters of the suppressor grid orbitron gauge (SGOG) are strongly dependent on the anode diameter in the 0.130 mm. to 0.025 mm. range.

5. The SGOG can be used as a pressure indicator down through the lower 10^{-12} torr range. Below this level the background currents appear to be too unstable for meaningful pressure measurements.

6. The gauge constant of the control orbitron gauge (COG) is strongly dependent on the radial position of the filament. Optimum response of the COG was observed for the 0.3R* filament position; three positions were studied, 0.3R, 0.5R, and 0.7R.

7. The response of the small orbitron gauge indicates that its primary usefulness lies in the 10^{-11} torr to 10^{-6} torr pressure range. This gauge is limited at the low pressure end by a positive background current which is assumed to be due to positive ions from the filament. Improved design perhaps could reduce this limitation.

8. It should be possible, using existing technology and without prohibitive expense, to set up calibration systems which can be used down into the 10^{-14} torr range.

---

* R is the radius of the suppressor grid in the SGOG and R is the radius of the ion collector in the COG.

APPENDIX A

ORBITRON GAUGE NONLINEARITY

The positive ion current obtained from operation of an orbitron gauge is not linearly related to the gas pressure. An attempt to explain this nonlinearity is made by considering three models for operation of the gauge.

Model I

In the simplest model, the orbitron gauge produces an ion current I^+ which is directly proportional to the product of the molecular density n, the mean path length $\bar{\ell}$, and the orbiting electron current I_e in the following manner,

$$I^+ = \sigma\, n\, \bar{\ell}\, I_e \quad . \tag{1}$$

By definition, n is directly proportional to the pressure p so that

$$I^+ = k\, \sigma\, p\, \bar{\ell}\, I_e \quad . \tag{2}$$

When one experimentally measures the quantities I^+, I_e and p, it is convenient to write

$$\bar{\ell} = k^{-1}\sigma^{-1}I_e^{-1}(I^+/p) \tag{3}$$

which becomes the definition of $\bar{\ell}$. The meaning of $\bar{\ell}$ is as follows: each electron which leaves the filament orbits independently about the anode, undergoes an indeterminant number of ionizing collisions, and eventually reaches the anode; $\bar{\ell}$ is the total path length traveled by the average electron.

If the orbitron operated exactly as described above, then a plot of $\bar{\ell}$, as defined in Eq. (3), versus p should yield a straight line with slope zero, i.e., a constant value. Experimental data, however, yield a curve which slowly increases between 10^{-10} torr and the mid-10^{-6} torr region; above 10^{-5} torr $\bar{\ell}$ rapidly decreases. It is easy to suggest two competing mechanisms which could account for such behavior. First, note that each ionizing collision also produces an electron which may then

orbit around the anode. Treating this electron as if it had originated at the filament, means that Eq. (2) must be altered to read

$$I^+ = k\,\sigma\,p\,\bar{\ell}\,I_e + k\,\sigma\,p\,\bar{\ell}\,(k\,\sigma\,p\,\bar{\ell}\,I_e)$$

$$= k\,\sigma\,p\,\bar{\ell}\,I_e\,(1 + k\,\sigma\,p\,\bar{\ell})$$

$$= k\,\sigma\,p\,I_e\,\bar{\ell}_1 \quad . \qquad (4)$$

where $\bar{\ell}_1$ is a "pressure dependent" mean path length. This pressure-dependent path length increases linearly with pressure. Second, it is obvious that as the pressure increases and the mean free path between ionizing collisions λ becomes comparable to the value of $\bar{\ell}_1$, the path length will be shortened. For example, an electron which originates with a potential energy of 450 eV, and loses 30 eV at each ionizing collison, could not under the most ideal conditions travel farther than 15 λ. A reasonable analytical form to use for the cut-off mentioned above is,

$$\frac{1}{\ell_d} = \frac{1}{\bar{\ell}} + \frac{1}{n\lambda} \quad , \qquad (5)$$

where ℓ_d is the decreased mean path length and n is the maximum permitted number of ionizing collisions. Families of p versus $\bar{\ell}$ curves, with n as a free parameter may be plotted. One may then calculate the pressure p_{MAX} at which the measured $\bar{\ell}$ maximizes and also the value of the ratio $r = \ell(p_{MAX})/\bar{\ell}(p_o)$ where $\bar{\ell}(p_o)$ is the pressure independent value of mean path length. For values of r which agree with experimental data (see Ref. 23), p_{MAX} is an order of magnitude too large. In order to have p_{MAX} in the mid-10^{-6} torr range as observed, n must be very nearly equal to 2.0, and r becomes very nearly unity, i.e., very slight departure from linearity.

Model II

The nonlinear pressure response of the orbitron gauge was first observed by Meyer who explained it[23] qualitatively as due to the space charge effect of positive gas ions in the vicinity of the filament. This point of view is based on the following hypothesis: the principal cause for loss of electrons from the orbiting volume (and consequent shortening of $\bar{\ell}$) is the perturbation of the field caused by the filament, which is biased some 30 V below the local potential. This perturbation appears as a "well"

to positive ions. As positive ions collect in this "well" they shield the filament and reduce the perturbation, which in turn increases ℓ . No quantitative calculations were made to justify this position.[23]

The following ball-park calculations were made in order to investigate the validity of the positive ion shielding mechanism. The charge on a cylindrical conductor at a potential V is

$$\lambda_q = \frac{2\pi\epsilon V}{\ln r_o/r_i} \text{ C/m} \quad , \tag{6}$$

where r_i is the radius of the conductor and r_o is the radius to the reference conductor. Because of the logarithm dependence, the charge is not very sensitive to the choice of r_o .

For the sake of argument we will assume the orbitron gauge to have the following set of parameters:

r_i (filament) = 6.3×10^{-5} m

r_o (perturbation) = 3×10^{-3} m

V (bias) = 50 V

x (length of filament) = 3×10^{-3} m

The total charge on such a filament will be about 2×10^{-12} C.

In order for the field lines to be distorted by space charge due to positive ions surrounding the filament, the space charge in a volume approximately as large as the region of distorted field lines must be greater than 1×10^{-13} C. This volume is less than $9 \times 10^{-7} m^3$ (a sphere whose diameter is one-half the radius of the orbitron). To find an approximate value of ion density in the orbitron volume, assume that positive ions are generated uniformly throughout the orbiting volume, have 100 ev energy and move in a straight line out of the orbiting volume.

The number of ions n^+ contained in a thin cylindrical shell at radius r (r = 0 at anode) is

$$n^+ = I^+\tau$$

$$= I^+ \frac{\Delta r}{\bar{v}} \qquad (7)$$

where τ is the time required for an ion to travel through the thin shell of thickness Δr with an average velocity $\bar{v} = [(2eV/m]^{1/2}$. The ion density at r is therefore,

$$\rho^+ = n^+/\Delta v \qquad (8)$$

where Δv is the shell volume. With these assumptions, the total available charge in the volume V_s surrounding the filament is

$$Q = \rho^+ V_s$$

$$= 7 \times 10^{-9}\ I^+ \quad . \qquad (9)$$

For typical values of sensitivity, 0.1 A/torr (N_2) , and for $p \sim 3 \times 10^{-6}$ torr, where $\bar{\ell}$ maximizes, $Q \sim 2 \times 10^{-15}$ C. This is three orders of magnitude smaller than the charge on the filament. Since the values chosen for sensitivity and volume surrounding the filament were larger than actual, the value of Q should be somewhat smaller. With the greatest strain of imagination one might expect the ions to have only about 1 eV energy near the filament; however, since the velocity goes as the square root of the energy, this would only increase the space charge by a factor of 10, still having it at least an order of magnitude too small to affect the filament bias. The only way to increase the density of positive ions would be to allow them to orbit about the filament; however, a quick calculation shows this to be impossible.

Model III

A third model was devised along the same line of attack as that presented in Eqs. (4) and (5), Model I, with a basic modification. For the moment, let us assume that instead of having all of the electrons which leave the filament execute orbits with all path lengths distributed about 6,000 cm.,* some large fraction (1-f) $\sim$ 95% go directly to the anode with

* From Ref. 23, the average path length measured to be about 6,000 cm. at low pressures.

a path length of $\sim$ 1 cm. and the other $\sim$ 5% (f), go into nearly perfect orbits with $\bar{\ell}_f \sim 120{,}000$ cm. so that $\bar{\ell} = 0.95 \times 1 + 0.05 \times 120{,}000 \sim 6{,}000$ cm. as measured. Let us further assume that most electrons produced by ionizing collisions will also have the same long path length $\bar{\ell}_f \sim 120{,}000$ cm. When these assumptions are used along with Eqs. (4) and (5) we find that by appropriate choices of F and n , one can fit the data almost exactly. Under this model, the terminology of Meyer,[23] i.e., "weak and strong coupling," becomes directly related to small and large values of f . "Weak coupling" then can be interpreted as that condition when very few electrons receive enough angular momentum to go into orbit, but those which do, go into extremely perfect orbits. The reason for nearly perfect orbits could be explained in the same manner that Meyer has explained weak coupling. "Strong coupling" means that most electrons go into mediocre orbits.

Although the agreement of the analytic function of the third model agrees well with the data, there is one obvious flaw which seriously injures the model. In an instrument built as crudely as the orbitron pump,[24] which operates at 250 watts, sufficient power is dissipated that one could see directly if 95% of the electrons went directly to the anode without orbiting. In fact, there is sufficient orbiting in the pump to distribute the electrons uniformly along the length of the anode. A second, less serious objection, would be to the assumption that all the electrons produced by an ionization go into long stable orbits of the same path length $\bar{\ell}_f$; obviously this path length must be shorter because they begin with less potential energy. Any reasonable alternative deposition of these electrons will leave the model essentially intact.

Let us return to the first objection. Basically the model is simply too extreme; i.e., that 95% go directly to the anode, while 5% have 120,000 cm. path lengths. This is unrealistic behavior. As in most other physical systems where large numbers of statistical events are possible, one expects some distribution over the entire space. It is difficult to construct or justify an analytical form of the distribution required, but it is not difficult to visualize such a distribution. One such distribution could be peaked about path lengths in the low hundreds of centimeters, perhaps containing 80% of all electrons between 100 and 500 cm. path lengths, 10% between 500 and 5,000 cm., 5% between 5,000 and 50,000 cm., and 5% between 50,000 and 200,000 cm. Further calculations at this point are prohibitive, and would have to be supported by experimental evidence which is too complex to obtain under this current program. However, one last observation will be made at this point to assist future efforts.

To support or disprove experimentally the positive ion shielding model, perform two experiments. Hold all parameters equal in both experiments but use two different gases. The measured $\bar{\ell}$ for the heaviest gas would begin to increase at an ion current lower than for the lighter gas by a ratio of $[m_1/m_2]^{1/2}$, where $m_1(m_2)$ is the molecular weight of the lighter (heavier) gas. This is due to the dependence upon the velocity of the ions. The results will not be a function of molecular weight if Model III is the correct model.

REFERENCES

1. F. P. Clay, Jr., and L. T. Melfi, Jr., J. Vac. Sci. Technol., 3, 167 (1966).

2. L. T. Melfi, Jr., J. Vac. Sci. Technol., 6(2), 322 (1969).

3. C. M. Gosselin, NASA Contractor Report NASA CR-1300 (NASA, Washington, D. C., 1969).

4. L. F. Kieffer and G. H. Dunn, Rev. of Mod. Phys., 38, 1 (1966).

5. W. B. Nottingham, Trans. 8th Nat'l. Symp., Am. Vac. Soc. (AVS, Pergammon Press, 1962), p. 494.

6. H. J. Schuetze and F. Stork, Vakuum, 11, 133 (1962).

7. J. P. Freytag and A. Schram, Nuovo Cim. Suppl., 1(2), 405 (1963).

8. P. A. Redhead, J. Vac. Sci. Technol., 6(5), 848 (1969).

9. J. Helmer and W. Hayward, Rev. Sci. Ins., 37, 1652 (1966).

10. P. A. Redhead, J. Vac. Sci. Technol., 3, 173 (1966).

11. W. D. Davis, Trans. Am. Vac. Soc., 363 (1962).

12. W. S. Lassiter, J. Vac. Sci. Technol., 6, 418 (1969).

13. F. Feakes and F. L. Torrey, Jr., Trans. Am. Vac. Soc., 257 (1963).

14. W. D. Davis, Trans. Am. Vac. Soc., 253 (1963).

15. W. J. Lange, J. H. Singleton, and D. P. Ericksin, J. Vac. Sci. Technol., 3, 338 (1966).

16. J. R. Young, J. Vac. Sci. Technol., 3, 345 (1966).

17. P. Bryant, W. W. Longley, and C. M. Gosselin, J. Vac. Sci. Technol., 3, 62 (1966).

18. P. Bryant and C. M. Gosselin, J. Vac. Sci. Technol., 3, 350 (1966).

19. R. W. Supple, NASA - Ames Research Center, Moffett Field, California. Paper given at Am. Vac. Society Meeting, 1967.

20. D. Pelz and G. Newton, J. Vac. Sci. Technol., 4, 239 (1967).

21. J. R. Roehrig and J. C. Simons, Trans. Am. Vac. Soc., 511 (1961).

22. C. F. Morrison, J. Vac. Sci. Technol., 4, 246 (1967).

23. E. A. Meyer and R. G. Herb, J. Vac. Sci. Technol., 4(2), 63 (1967).

24. J. C. Maliakal, et al., J. Vac. Sci. Technol., 1(2), 54 (1964).